

---

# Communication-Efficient Personalized Adaptation via Federated-Local Model Merging

---

Yinan Zou<sup>1</sup> Md Kamran Chowdhury Shisher<sup>1</sup> Christopher G. Brinton<sup>1</sup> Vishrant Tripathi<sup>1</sup>

## Abstract

Parameter-efficient fine-tuning methods, such as LoRA, offer a practical way to adapt large vision and language models to client tasks. However, this becomes particularly challenging under task-level heterogeneity in federated deployments. In this regime, personalization requires balancing *general knowledge* with *personalized knowledge*, yet existing approaches largely rely on heuristic mixing rules and lack theoretical justification. Moreover, prior model merging approaches are also computation and communication intensive, making the process inefficient in federated settings. In this work, we propose POTARA, a principled framework for federated personalization that constructs a personalized model for each client by merging two complementary models: (i) a federated model capturing *general knowledge*, and (ii) a local model capturing *personalized knowledge*. Through the construct of linear mode connectivity, we show that the expected task loss admits a variance trace upper bound, whose minimization yields closed-form optimal mixing weights that guarantee a tighter bound for the merged model than for either the federated or local model alone. Experiments on vision and language benchmarks show that POTARA consistently improves personalization while reducing communication, leading to a strong performance-communication trade-off.

## 1. Introduction

Large vision models (LVMs) and large language models (LLMs) have achieved remarkable progress, enabling their widespread adoption across diverse downstream applications (Zhao et al., 2023; Awais et al., 2025). Adapting pre-trained models to domain specific tasks typically requires fine-tuning on task relevant data, but full parameter

fine-tuning is computationally expensive and impractical at scale. To mitigate this cost, parameter-efficient fine-tuning methods have been developed, among which low-rank adaptation (LoRA) (Hu et al., 2022) has become particularly popular. Domain specific fine-tuning of large models often requires large heterogeneous datasets which are typically split across organizations and cannot be centralized due to privacy and security constraints. Federated learning (FL) (McMahan et al., 2017) addresses this issue by enabling collaborative training while keeping raw data local.

Federated large model fine-tuning (Zhang et al., 2024) integrates FL with LoRA, allowing clients to update and communicate only LoRA modules while jointly learning a global model. Despite its promise, federated LoRA fine-tuning faces pronounced *task heterogeneity*: different clients may pursue distinct, and sometimes even conflicting, objectives. In such settings, the knowledge required by each client naturally decomposes into two complementary components: (i) *general knowledge* that can be transferred across clients and tasks, and (ii) *personalized knowledge* that is specific to each client’s local data and task.

**Challenges.** A central challenge is how to balance cross-client *general knowledge* and client-specific *personalized knowledge*. It remains unclear, from a principled theoretical perspective, how much emphasis should be placed on general versus personalized knowledge when forming the final client model. Although recent methods attempt to provide a solution (Yang et al., 2024; Bian et al., 2026), they lack theoretical justification, leaving a gap for theoretically-grounded solutions. Additionally, communication is the primary bottleneck in FL, and LoRA-based training still requires the repeated transmission of parameters across many rounds. These considerations call for an approach that (i) explicitly control the general-personalized trade-off in a principled manner and (ii) achieve favorable performance-communication trade-off in realistic federated deployments.

### 1.1. Contributions

Motivated by these limitations, this work aims to develop a framework for efficient federated fine-tuning under task heterogeneity. Our key contributions are as follows:

<sup>1</sup>Elmore Family School of Electrical and Computer Engineering, Purdue University. Correspondence to: Yinan Zou <zou211@purdue.edu>.

- We propose POTARA<sup>1</sup>, a federated LoRA personalization framework to jointly (i) achieve an effective trade-off between federation and personalization, and (ii) balance communication efficiency with performance. POTARA constructs a personalized model for each client by merging two complementary models: a collaborative federated model that captures *general knowledge* across all clients, and a local fine-tuning model that emphasizes *personalized knowledge*.
- To determine the mixing weight between the federated model and the local model, we develop a rigorous analysis grounded in linear mode connectivity (LMC). We show that, within an LMC basin around the optimum, the expected excess task losses of the federated model, the local model, and their merged model admits an upper bound in which the key term is a variance trace (see Theorem 3.6). Minimizing this bound yields closed-form optimal mixing weights, which guarantee that the merged model achieves the tighter bound than both the federated model and the local model (see Lemma 3.7).
- We conduct extensive experiments on vision and language benchmarks. The experimental results show that our method achieves superior performance compared to baseline methods while significantly reducing communication overhead, thereby offering a favorable performance-communication trade-off.

## 1.2. Related Work

**Model Merging.** Model merging aims to combine multiple task-specific models into a single model without additional training. Wortsman et al. (2022) utilized averaged parameters to construct the merged model. To account for parameter importance, Matena & Raffel (2022) proposed weighted fusion, where merging weights are derived from the Fisher information matrix (Fisher, 1922). Jin et al. (2023) formulated model merging as a linear regression problem and obtained a closed-form solution. Instead of averaging weights, Ilharco et al. (2023) introduced task vectors by subtracting the pre-trained parameters from each fine-tuned model, and then linearly combining these task vectors to form a merged model. Yadav et al. (2023) proposed to reduce conflicts in task vectors (Ilharco et al., 2023) by trimming low-magnitude updates, resolving sign disagreements, and merging disjoint parameter subsets with consistent signs. Yu et al. (2024) further explored this issue by randomly dropping a subset of fine-tuned weights and rescaling the remainder, yielding sparse task vectors that alleviate destructive interference. Most existing methods (Ilharco et al., 2023; Yadav et al., 2023; Yu et al., 2024; Qi et al., 2025;

Stoica et al., 2025) select merging weights via heuristic tuning (e.g., grid search), which is computation intensive. In contrast, our approach derives the optimal mixing weights from theory, substantially improving efficiency by eliminating expensive per-client weight sweeps and repeated evaluations.

**Personalized Federated Learning.** Personalized federated learning aims to overcome the limitation of a single global model by adapting client models to their local data distribution (Tan et al., 2022). Common approaches include meta learning (Fallah et al., 2020; Chen et al., 2018), partial model personalization (Collins et al., 2021; Pillutla et al., 2022), multi-task learning (Smith et al., 2017; Li et al., 2021), hypernetworks (Shamsian et al., 2021), and clustering (Duan et al., 2021; Ghosh et al., 2020). A related study on personalized FL and model merging, FedMerge (Chen et al., 2026), proposed a multi-model FL framework in which the server maintains a pool of global models, and each client obtains a personalized model by merging these server-side models. However, the server stores multiple global models and perform gradient-based updates for each model in the pool, both the storage and computation overhead on the server scale linearly with the number of global models. In contrast, our method follows a single-model paradigm where the server maintains only one global model and the server only needs to average the local models, making it substantially more resource efficient for large model fine-tuning. Moreover, the above methods primarily address statistical heterogeneity (e.g., label distribution skew) and are typically evaluated on conventional small model architectures. In contrast, we study a more realistic and challenging regime for large model adaptation, where heterogeneity manifests not only in label diversity but also in task diversity across clients.

**Federated Fine-Tuning.** FedIT (Zhang et al., 2024) integrated LoRA with FedAvg and is one of the earliest efforts to combine parameter-efficient adaptation with federated optimization. Subsequent works studied federated LoRA under differential privacy (Sun et al., 2024), the asymmetric roles of LoRA matrices (Guo et al., 2025), and heterogeneous-rank LoRA matrices (Fang et al., 2025; Cho et al., 2024; Bai et al., 2024; Wang et al., 2024). Hao et al. (2025); Qi et al. (2024) studied personalization under label-distribution heterogeneity while still assuming task-homogeneous adaptation. Considering task heterogeneity, Yang et al. (2024); Bian et al. (2026) introduced global and local LoRA modules and combine them via a dynamic mixer. Although empirically effective, such designs lack theoretical justification for determining the appropriate mixing weights between these two LoRA modules. In contrast, our method derives the optimal mixing weight from a principled theoretical analysis.

<sup>1</sup>POTARA derives its name from the Potara fusion in Dragon Ball, where two independent entities are merged into a single, and more powerful form.

## 2. Preliminaries and Notation

In this section, we introduce the preliminary concepts and notation used throughout the paper, including LoRA, federated fine-tuning, and linear mode connectivity.

### 2.1. Parameter-Efficient Fine-Tuning: LoRA

Consider a pre-trained model with parameters  $\mathbf{W}_{\text{Pre}} \in \mathbb{R}^{m \times n}$ . We denote  $\Delta \mathbf{W} \in \mathbb{R}^{m \times n}$  as the trainable update matrix during fine-tuning. Instead of updating all parameters in  $\Delta \mathbf{W}$ , LoRA (Hu et al., 2022) decomposes  $\Delta \mathbf{W}$  into two low-rank matrices  $\mathbf{A} \in \mathbb{R}^{r \times n}$  and  $\mathbf{B} \in \mathbb{R}^{m \times r}$ , where  $r \ll \min(m, n)$ . This decomposition allows the fine-tuning to focus on the significantly smaller low-rank matrices  $\mathbf{A}$  and  $\mathbf{B}$  instead of the full matrix  $\Delta \mathbf{W}$ . Consequently, the total number of trainable parameters is reduced from  $m \times n$  to  $r \times (m + n)$ . The model parameters after fine-tuning are given by:

$$\mathbf{W}_{\text{FT}} = \mathbf{W}_{\text{Pre}} + \Delta \mathbf{W} = \mathbf{W}_{\text{Pre}} + \mathbf{B}\mathbf{A}, \quad (1)$$

where  $\mathbf{A}$  is typically initialized with random Gaussian values and  $\mathbf{B}$  is initialized to zero (Hu et al., 2022; Hayou et al., 2024).

### 2.2. Federated LoRA Fine-Tuning

FedIT (Zhang et al., 2024) integrates LoRA (Hu et al., 2022) with the FedAvg (McMahan et al., 2017) framework. The procedure of FedIT is summarized in Algorithm 1. FedIT aims to minimize a global loss function subject to the consensus constraints  $\mathbf{B}^{(1)} = \dots = \mathbf{B}^{(N)}$  and  $\mathbf{A}^{(1)} = \dots = \mathbf{A}^{(N)}$  where  $\mathbf{B}^{(i)}$  and  $\mathbf{A}^{(i)}$  denotes the LoRA matrices at client  $i$ . Consequently, it ultimately yields a single model shared across all clients.

---

#### Algorithm 1 FedIT

---

- 1: **Initialize:** Per-trained model  $\mathbf{W}_{\text{Pre}}$ , initialized LoRA modules  $\{\mathbf{B}^0, \mathbf{A}^0\}$ ;
- 2: **for** communication round  $t = 0, 1, \dots, T - 1$  **do**
- 3: Server broadcasts the current global LoRA modules  $\{\mathbf{B}^t, \mathbf{A}^t\}$  to all clients.
- 4: **for** each client  $i = 1, \dots, N$  in parallel **do**
- 5: Client  $i$  keeps pre-trained model  $\mathbf{W}_{\text{Pre}}$  frozen and updates only LoRA modules to obtain  $\{\mathbf{B}^{(i),t}, \mathbf{A}^{(i),t}\}$ .
- 6: Client  $i$  uploads its local LoRA modules  $\{\mathbf{B}^{(i),t}, \mathbf{A}^{(i),t}\}$  to the server.
- 7: **end for**
- 8: Server updates the global LoRA modules via

$$\mathbf{B}^{(i),t+1} = \frac{1}{N} \sum_{i=1}^N \mathbf{B}^{(i),t}, \mathbf{A}^{(i),t+1} = \frac{1}{N} \sum_{i=1}^N \mathbf{A}^{(i),t}.$$

- 9: **end for**
- 

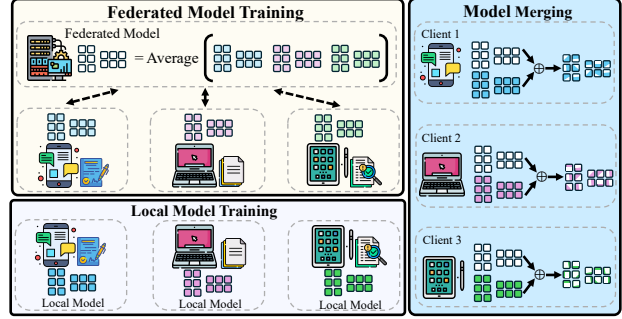


Figure 1. Illustration of POTARA. We train a FedIT model via FL and train local fine-tuning models. We obtain the final personalized model by weighted merging these FedIT and local models.

### 2.3. Linear Mode Connectivity

Prior works (Draxler et al., 2018; Garipov et al., 2018) show that the minima found by two independently trained neural networks can be connected by a simple path along which the loss or accuracy remains nearly constant. This phenomenon is referred to as mode connectivity. Subsequent studies (Nagarajan & Kolter, 2019; Frankle et al., 2020) further show that when neural networks are trained from the same initialization, the resulting well-trained models can be connected by a linear path, known as linear mode connectivity (LMC). We restate the definition of LMC used in (Frankle et al., 2020; Zhou et al., 2023).

**Definition 2.1.** (Frankle et al., 2020; Zhou et al., 2023) Given a dataset  $\mathcal{D}$  and two well-trained models  $\mathbf{W}_1$  and  $\mathbf{W}_2$  such that  $f(\mathbf{W}_1; \mathcal{D}) \approx f(\mathbf{W}_2; \mathcal{D})$ , we say that  $\mathbf{W}_1$  and  $\mathbf{W}_2$  are linearly connected if they satisfy

$$f(\lambda_1 \mathbf{W}_1 + \lambda_2 \mathbf{W}_2; \mathcal{D}) \approx f(\mathbf{W}_1; \mathcal{D}), \quad \forall \lambda_1, \lambda_2 \geq 0, \lambda_1 + \lambda_2 = 1, \quad (2)$$

where  $f(\mathbf{W}; \mathcal{D})$  denotes the loss of model  $\mathbf{W}$  on dataset  $\mathcal{D}$ .

In Definition 2.1, two models  $\mathbf{W}_1$  and  $\mathbf{W}_2$  are linearly connected if the loss of the interpolated mode remains nearly unchanged. In other words,  $\mathbf{W}_1$  and  $\mathbf{W}_2$  lie within the same flat basin of the loss landscape, and their linear interpolation remains inside this basin (Neysshabur et al., 2020).

## 3. Our Method: POTARA

In this section, we propose POTARA, which achieves a principled trade-off between federation and personalization while simultaneously balancing communication efficiency and performance.

### 3.1. Motivation

In large model fine-tuning, different clients usually hold data from distinct tasks (e.g., question classification versus sentiment analysis) (Fallah et al., 2020; Collins et al.,

2021; Bian et al., 2026; Yang et al., 2024; Tian et al., 2023). In such task-heterogeneous settings, consensus-based FL methods often underperform, since enforcing a single shared solution neglects both task diversity and the need for client-specific adaptation. A trivial alternative is to let each client fine-tune independently without communication. However, the number of local data samples is typically insufficient to train a satisfactory model in practical settings. By exchanging information across clients, each client can exploit transferable knowledge learned elsewhere to improve its own model. Accordingly, personalized federated fine-tuning aims to learn a client-specific model that effectively combines *general knowledge* across clients with *personalized knowledge* adapted to the client’s local task.

### 3.2. Federated-Local Model Merging

Model merging provides a lightweight mechanism for combining complementary capabilities from multiple fine-tuned models without additional joint training. Building on this idea, we propose POTARA, which constructs a personalized model for each client by merging two complementary models:

- a collaborative FedIT model learned through cross-client communication,
- a purely local model fine-tuned only on that client’s data.

Intuitively, the FedIT model captures *general knowledge* distilled from all clients. In contrast, the local model emphasizes *personalized knowledge* tailored to the client’s task and distribution. By merging them, POTARA yields a client-specific model that simultaneously leverages federation and personalization, offering an effective trade-off between these two objectives.

Specifically, we denote the task vector (Ilharco et al., 2023) of client  $i$ ’s locally fine-tuned model as  $\boldsymbol{\theta}_{\text{Local}}^{(i)} = \mathbf{B}_{\text{Local}}^{(i)} \mathbf{A}_{\text{Local}}^{(i)}$ , and the task vector of the FedIT model as  $\boldsymbol{\theta}_{\text{FedIT}} = \mathbf{B}_{\text{FedIT}} \mathbf{A}_{\text{FedIT}}$ . For each client  $i$ , we form the merged task vector by a convex combination:

$$\boldsymbol{\theta}_{\text{Merge}}^{(i)} = \lambda_{\text{FedIT}}^{(i)} \boldsymbol{\theta}_{\text{FedIT}} + \lambda_{\text{Local}}^{(i)} \boldsymbol{\theta}_{\text{Local}}^{(i)}, \quad (3)$$

where  $\lambda_{\text{FedIT}}^{(i)}, \lambda_{\text{Local}}^{(i)} \geq 0$  denote the mixing weights for client  $i$  and  $\lambda_{\text{FedIT}}^{(i)} + \lambda_{\text{Local}}^{(i)} = 1$ . Then, the final model for each client is given by

$$\mathbf{W}_{\text{Final}}^{(i)} = \mathbf{W}_{\text{Pre}} + \boldsymbol{\theta}_{\text{Merge}}^{(i)}. \quad (4)$$

A natural question then arises: how to choose the mixing weights  $\lambda_{\text{FedIT}}^{(i)}$  and  $\lambda_{\text{Local}}^{(i)}$ ? This choice is critical, as it governs the trade-off between leveraging *general knowledge*

from FedIT and preserving *personalized knowledge* from local fine-tuning. Next, we present our weighting strategy for determining  $\lambda_{\text{FedIT}}^{(i)}$  and  $\lambda_{\text{Local}}^{(i)}$  in a principled manner.

### 3.3. Determination of Mixing Weights

In the preliminaries, we recalled the standard definition of LMC, which characterizes the phenomenon in terms of the loss remaining nearly constant along the linear interpolation path. To obtain a local geometric characterization of LMC, we introduce the notion of LMC basin below.

**Definition 3.1.** For a given radius  $\delta > 0$ , define the LMC basin around the optimum  $\mathbf{W}^*$  as

$$\mathcal{U}_\delta = \{\mathbf{W} : \|\mathbf{W} - \mathbf{W}^*\| \leq \delta\}. \quad (5)$$

Two models  $\mathbf{W}_1$  and  $\mathbf{W}_2$  exhibit linear mode connectivity in  $\mathcal{U}_\delta$  if all their convex combination lies entirely in  $\mathcal{U}_\delta$ , i.e.,

$$\lambda_1 \mathbf{W}_1 + \lambda_2 \mathbf{W}_2 \in \mathcal{U}_\delta, \quad \forall \lambda_1, \lambda_2 \geq 0, \lambda_1 + \lambda_2 = 1. \quad (6)$$

We assume that the FedIT and each local model exhibit LMC within the LMC basin, i.e., the entire linear interpolation path between them remains inside the basin.

**Assumption 3.2.** Let  $\mathcal{U}_\delta$  be the LMC basin in Definition 3.1.

For each client  $i$ , we assume that  $\mathbf{W}_{\text{Pre}} + \lambda_{\text{FedIT}}^{(i)} \boldsymbol{\theta}_{\text{FedIT}} + \lambda_{\text{Local}}^{(i)} \boldsymbol{\theta}_{\text{Local}}^{(i)} \in \mathcal{U}_\delta$ ,  $\forall \lambda_{\text{FedIT}}^{(i)}, \lambda_{\text{Local}}^{(i)} \geq 0$ ,  $\lambda_{\text{FedIT}}^{(i)} + \lambda_{\text{Local}}^{(i)} = 1$ .

Throughout our analysis, we focus on the behavior of the loss landscape within the LMC basin and make the following standard assumptions on optimization.

**Assumption 3.3.** The task loss function  $\mathcal{L}$  is locally Lipschitz smooth within the LMC basin  $\mathcal{U}_\delta$ . There exist constants  $L > 0$  such that

$$\mathcal{L}(\mathbf{y}) \leq \mathcal{L}(\mathbf{x}) + \nabla \mathcal{L}(\mathbf{x})^\top (\mathbf{y} - \mathbf{x}) + \frac{L}{2} \|\mathbf{y} - \mathbf{x}\|^2, \quad \forall \mathbf{x}, \mathbf{y} \in \mathcal{U}_\delta. \quad (7)$$

Equivalently, the Hessian of  $\mathcal{L}$  is bounded within the LMC basin, i.e.,  $\nabla^2 \mathcal{L}(\mathbf{x}) \preceq L \mathbf{I}$ ,  $\forall \mathbf{x} \in \mathcal{U}_\delta$ .

**Assumption 3.4.** (Nesterov & Polyak, 2006; Carmon et al., 2018) The Hessian of the task loss within the LMC basin is  $L_H$ -Lipschitz continuous if  $\|\nabla^2 \mathcal{L}(\mathbf{y}) - \nabla^2 \mathcal{L}(\mathbf{x})\| \leq L_H \|\mathbf{y} - \mathbf{x}\|$ ,  $\forall \mathbf{x}, \mathbf{y} \in \mathcal{U}_\delta$ , where  $L_H > 0$  is a constant.

In the following, we show that the model obtained by merging the FedIT model and the local model yields a personalized performance gain. For clarity, we omit the client index.

We use the Laplace approximation to approximate the task vectors of FedIT (i.e.,  $\boldsymbol{\theta}_{\text{FedIT}}$ ) and local fine-tuning (i.e.,

$\theta_{\text{Local}}$ ) as Gaussian distributions:

$$\theta_{\text{FedIT}} \sim \mathcal{N}(\boldsymbol{\mu}_{\text{FedIT}}, \boldsymbol{\Sigma}_{\text{FedIT}}), \quad (8)$$

$$\theta_{\text{Local}} \sim \mathcal{N}(\boldsymbol{\mu}_{\text{Local}}, \boldsymbol{\Sigma}_{\text{Local}}), \quad (9)$$

where  $\boldsymbol{\mu}_{\text{FedIT}}$  and  $\boldsymbol{\mu}_{\text{Local}}$  denote the MAP parameter estimates of the corresponding task vectors, and  $\boldsymbol{\Sigma}_{\text{FedIT}} = \mathbf{F}_{\boldsymbol{\mu}_{\text{FedIT}}}^{-1}$  and  $\boldsymbol{\Sigma}_{\text{Local}} = \mathbf{F}_{\boldsymbol{\mu}_{\text{Local}}}^{-1}$  are given by the inverses of their Fisher information matrices. The full derivation is provided in Appendix A.1.

We further assume a joint Gaussian distribution of FedIT and local task vectors, which introduces an explicit cross-covariance term.

**Assumption 3.5.** (Wang et al., 2025) We assume that  $(\theta_{\text{FedIT}}, \theta_{\text{Local}})$  follow a joint Gaussian distribution:

$$\begin{bmatrix} \theta_{\text{FedIT}} \\ \theta_{\text{Local}} \end{bmatrix} \sim \mathcal{N}\left(\begin{bmatrix} \boldsymbol{\mu}_{\text{FedIT}} \\ \boldsymbol{\mu}_{\text{Local}} \end{bmatrix}, \begin{bmatrix} \boldsymbol{\Sigma}_{\text{FedIT}} & \boldsymbol{\Sigma}_{\text{Cross}} \\ \boldsymbol{\Sigma}_{\text{Cross}}^{\top} & \boldsymbol{\Sigma}_{\text{Local}} \end{bmatrix}\right), \quad (10)$$

where  $\boldsymbol{\Sigma}_{\text{Cross}}$  denotes the cross-covariance matrix between the two task vectors. We assume that FedIT task and local task are correlated, therefore, the cross-covariance matrix satisfies  $\boldsymbol{\Sigma}_{\text{Cross}} \succeq 0$ . Furthermore, we assume that  $\boldsymbol{\Sigma}_{\text{Cross}} \preceq \boldsymbol{\Sigma}_{\text{FedIT}}$  and  $\boldsymbol{\Sigma}_{\text{Cross}} \preceq \boldsymbol{\Sigma}_{\text{Local}}$ .

The conditions  $\boldsymbol{\Sigma}_{\text{Cross}} \preceq \boldsymbol{\Sigma}_{\text{FedIT}}$  and  $\boldsymbol{\Sigma}_{\text{Cross}} \preceq \boldsymbol{\Sigma}_{\text{Local}}$  indicate that the cross-covariance is not larger than the marginal variances, i.e., the shared uncertainty does not dominate each model's own uncertainty.

With the joint Gaussian model in Assumption 3.5, we can derive the Gaussian distribution of the merged task vector:

$$\theta_{\text{Merge}} \sim \mathcal{N}(\boldsymbol{\mu}_{\text{Merge}}, \boldsymbol{\Sigma}_{\text{Merge}}), \quad (11)$$

where

$$\boldsymbol{\mu}_{\text{Merge}} = \lambda_{\text{FedIT}} \boldsymbol{\mu}_{\text{FedIT}} + \lambda_{\text{Local}} \boldsymbol{\mu}_{\text{Local}}, \quad (12)$$

$$\begin{aligned} \boldsymbol{\Sigma}_{\text{Merge}} &= \lambda_{\text{FedIT}}^2 \boldsymbol{\Sigma}_{\text{FedIT}} + \lambda_{\text{Local}}^2 \boldsymbol{\Sigma}_{\text{Local}} \\ &+ \lambda_{\text{FedIT}} \lambda_{\text{Local}} (\boldsymbol{\Sigma}_{\text{Cross}} + \boldsymbol{\Sigma}_{\text{Cross}}^{\top}). \end{aligned} \quad (13)$$

We now present an expected excess loss bound for FedIT, Local, and their merged model.

**Theorem 3.6.** Under Definition 3.1, Assumption 3.2, 3.3, 3.4, and 3.5, for  $i \in \{\text{FedIT}, \text{Local}, \text{Merge}\}$ , it holds that

$$\begin{aligned} \mathbb{E}[\mathcal{L}(\mathbf{W}_{\text{Pre}} + \theta_i) - \mathcal{L}(\mathbf{W}^*)] &\leq \left(\frac{L}{2} + \frac{L_H}{6} \delta\right) \delta^2 \\ &+ \left(\frac{L}{2} + \frac{L_H}{6} \delta\right) \text{tr}(\boldsymbol{\Sigma}_i). \end{aligned} \quad (14)$$

**Proof sketch of Theorem 3.6.** To bound the expected excess loss, we expand  $\mathcal{L}$  around the optimum  $\mathbf{W}^*$ . Let

$\phi = \mathbf{W}_{\text{Pre}} + \theta_{\text{Merge}} - \mathbf{W}^*$  and  $\mathbf{H} = \nabla^2 \mathcal{L}(\mathbf{W}^*)$ . By Lemma 2.2 in (Carmon et al., 2018), we have

$$\mathcal{L}(\mathbf{W}_{\text{Pre}} + \theta_{\text{Merge}}) \leq \mathcal{L}(\mathbf{W}^*) + \frac{1}{2} \phi^{\top} \mathbf{H} \phi + \frac{L_H}{6} \|\phi\|_2^3. \quad (15)$$

By  $\mathbb{E}[\phi^{\top} \mathbf{H} \phi] = (\mathbb{E} \phi)^{\top} \mathbf{H} (\mathbb{E} \phi) + \text{tr}(\mathbf{H} \text{Cov}(\phi))$ , we obtain

$$\begin{aligned} &\mathbb{E}[\mathcal{L}(\mathbf{W}_{\text{Pre}} + \theta_{\text{Merge}}) - \mathcal{L}(\mathbf{W}^*)] \\ &\leq \frac{1}{2} (\mathbf{W}_{\text{Pre}} + \boldsymbol{\mu}_{\text{Merge}} - \mathbf{W}^*)^{\top} \mathbf{H} (\mathbf{W}_{\text{Pre}} + \boldsymbol{\mu}_{\text{Merge}} - \mathbf{W}^*) \\ &\quad + \frac{1}{2} \text{tr}(\mathbf{H} \boldsymbol{\Sigma}_{\text{Merge}}) + \frac{L_H}{6} \mathbb{E} \|\phi\|_2^3. \end{aligned} \quad (16)$$

Due to  $\|\phi\|_2 \leq \delta$ , we have  $\|\phi\|_2^3 \leq \delta \|\phi\|_2^2$  and hence  $\mathbb{E} \|\phi\|_2^3 \leq \delta \mathbb{E} \|\phi\|_2^2$ . Moreover,  $\mathbb{E} \|\phi\|_2^2 = \|\mathbb{E} \phi\|_2^2 + \text{tr}(\text{Cov}(\phi)) = \|\mathbf{W}_{\text{Pre}} + \boldsymbol{\mu}_{\text{Merge}} - \mathbf{W}^*\|_2^2 + \text{tr}(\boldsymbol{\Sigma}_{\text{Merge}})$ . Finally, using  $\mathbf{H} \preceq L\mathbf{I}$  yields the bound in terms of  $\delta^2$  and  $\text{tr}(\boldsymbol{\Sigma}_{\text{Merge}})$ . The same argument applies to  $\theta_{\text{FedIT}}$  and  $\theta_{\text{Local}}$  individually. The full derivation is provided in Appendix A.2.  $\square$

Theorem 3.6 indicates that the excess loss upper bound is primarily controlled by the trace term. For the merged model,  $\text{tr}(\boldsymbol{\Sigma}_{\text{Merge}})$  depends on the mixing weights  $(\lambda_{\text{FedIT}}, \lambda_{\text{Local}})$ . In the following, we minimize this trace term to obtain the optimal mixing weights in closed form.

**Lemma 3.7.** Minimizing the trace term  $\text{tr}(\boldsymbol{\Sigma}_{\text{Merge}})$  yields the optimal mixing weights, given by

$$\lambda_{\text{FedIT}}^* = \frac{b - c}{a + b - 2c}, \quad \lambda_{\text{Local}}^* = \frac{a - c}{a + b - 2c}, \quad (17)$$

where  $a = \text{tr}(\boldsymbol{\Sigma}_{\text{FedIT}})$ ,  $b = \text{tr}(\boldsymbol{\Sigma}_{\text{Local}})$ ,  $c = \text{tr}(\boldsymbol{\Sigma}_{\text{Cross}})$ . At this optimum, the merged trace is smaller than those of the two individual models:

$$\text{tr}(\boldsymbol{\Sigma}_{\text{Merge}}) \leq \min\{\text{tr}(\boldsymbol{\Sigma}_{\text{FedIT}}), \text{tr}(\boldsymbol{\Sigma}_{\text{Local}})\}. \quad (18)$$

At the optimal weights  $(\lambda_{\text{FedIT}}^*, \lambda_{\text{Local}}^*)$  in Lemma 3.7,  $\text{tr}(\boldsymbol{\Sigma}_{\text{Merge}})$  attains its minimum. Moreover, this minimum satisfies  $\text{tr}(\boldsymbol{\Sigma}_{\text{Merge}}) \leq \min\{\text{tr}(\boldsymbol{\Sigma}_{\text{FedIT}}), \text{tr}(\boldsymbol{\Sigma}_{\text{Local}})\}$ . Therefore, by Theorem 3.6 and Lemma 3.7, the merged model admits an excess loss upper bound that is tighter than the bounds for FedIT or local fine-tuning alone.

### 3.4. Estimation of Fisher Information Matrix

In Section 3.3, we established that  $\boldsymbol{\Sigma}_{\text{FedIT}} = \mathbf{F}_{\boldsymbol{\mu}_{\text{FedIT}}}^{-1}$  and  $\boldsymbol{\Sigma}_{\text{Local}} = \mathbf{F}_{\boldsymbol{\mu}_{\text{Local}}}^{-1}$ , i.e., each posterior variance is given by the inverse Fisher information matrix. To reduce the computation cost, we adopt a diagonal approximation of the Fisher information matrix (Matena & Raffel, 2022). The diagonal Fisher matrix evaluated at the posterior mean  $\boldsymbol{\mu}_i$  is given by

$$\hat{\mathbf{F}}_{\boldsymbol{\mu}_i} = \text{diag}\left(\frac{1}{N} \sum_{n=1}^N \mathbb{E}_{\mathbf{y} \sim p_{\boldsymbol{\mu}_i}(\mathbf{y}|\mathbf{x}_n)} \left[ \left( \nabla_{\boldsymbol{\mu}_i} \log p_{\boldsymbol{\mu}_i}(\mathbf{y}|\mathbf{x}_n) \right)^{\odot 2} \right]\right), \quad (19)$$

where  $N$  is the mini-batch size to estimate the Fisher information and  $(\cdot)^{\odot 2}$  denotes the element-wise square operator. Consequently, the posterior variance can be approximated as  $\Sigma_i \approx (\hat{\mathbf{F}}_{\mu_i})^{-1}$ .

To approximate the cross-covariance between the two task vectors, we compute per-sample gradients under  $\mu_{\text{FedIT}}$  and  $\mu_{\text{Local}}$ , estimate their coordinate-wise variances and covariance, and obtain a gradient correlation coefficient  $\rho_k$  for each parameter dimension. We then construct a diagonal approximation

$$(\Sigma_{\text{Cross}})_{kk} \approx \rho_k \sqrt{(\Sigma_{\text{FedIT}})_{kk}(\Sigma_{\text{Local}})_{kk}}, \quad (20)$$

where  $k$  denotes the parameter coordinate and  $\rho_k$  is clipped to ensure  $\Sigma_{\text{Cross}} \succeq 0$  and  $\Sigma_{\text{Cross}} \preceq \Sigma_{\text{FedIT}}, \Sigma_{\text{Local}}$ . Further details on the estimation procedure and computation times are provided in the Appendix B and F.

### 3.5. Communication Overhead Comparison

We denote  $T$  as the number of communication rounds. FedIT (Zhang et al., 2024) uploads both **A** and **B** each round, yielding per-client overhead  $\mathcal{O}(r(m+n)T)$ . FedSA (Guo et al., 2025) uploads only **A**, yielding  $\mathcal{O}(rnT)$ . FFA-LoRA (Sun et al., 2024) uploads only **B**, yielding  $\mathcal{O}(rmT)$ . FedDPA (Yang et al., 2024) uploads one of two locally trained LoRA modules per round, yielding  $\mathcal{O}(r(m+n)T)$ . FedALT (Bian et al., 2026) uploads the local LoRA module each round, yielding  $\mathcal{O}(r(m+n)T)$ . For POTARA, clients upload both **A** and **B** only during the FedIT phase, so the overhead is  $\mathcal{O}(r(m+n)T_{\text{FedIT}})$ , where  $T_{\text{FedIT}}$  denotes the number of communication rounds required to train the FedIT model. The communication overhead comparison is summarized in Table 1. POTARA achieves consistent performance gains even under a reduced communication budget. A detailed performance-communication trade-off is reported in Section 4.3.

Table 1. Communication Overhead Comparison.

Method	Communication Overhead
FedIT	$\mathcal{O}(r(m+n)T)$
FedSA	$\mathcal{O}(rnT)$
FFA-LoRA	$\mathcal{O}(rmT)$
FedALT	$\mathcal{O}(r(m+n)T)$
FedDPA	$\mathcal{O}(r(m+n)T)$
POTARA	$\mathcal{O}(r(m+n)T_{\text{FedIT}})$

## 4. Experiments

In this section, we evaluate and compare the performance of the proposed POTARA against baseline methods on vision and language benchmarks. The baseline methods include Local fine-tuning (Hu et al., 2022), FedIT (Zhang et al., 2024), FFA-LoRA (Sun et al., 2024), FedSA (Guo et al., 2025), FedDPA (Yang et al., 2024), FedALT (Bian et al.,

2026), and Fisher Merging (Matena & Raffel, 2022).

### 4.1. Vision Benchmark

We adopt ViT-B/16 (Dosovitskiy et al., 2021) as the pre-trained model. To simulate label heterogeneity, we partition CIFAR-100 across clients using a Dirichlet distribution with concentration parameter  $\alpha = 0.5$ . For each client, we construct both the training and test splits according to the same Dirichlet-based partition. Unless otherwise specified, we consider 10 clients. All federated baselines are trained for 600 communication rounds. For both Fisher merging and the proposed POTARA, we first train the FedIT model and the local fine-tuning model for 400 and 300 rounds, respectively, and then merge the two models to obtain the final model. As shown in Table 2, the proposed POTARA achieves the best overall performance among all baseline methods, outperforming the strongest baseline, FedDPA, by an average accuracy margin of 3.41. Moreover, POTARA reduces the communication cost by 33.3% compared to FedDPA, FedALT, and FedIT. See Section 4.3 and Figure 2a for a detailed performance-communication trade-off analysis.

### 4.2. Language Benchmark

We next evaluate POTARA on LLM and NLP benchmark. We adopt LLaMA-3.2-3B-Instruct (Dubey et al., 2024) as the pre-trained model and construct a task-heterogeneous setting by assigning each client a distinct task from the commonsense reasoning benchmark (Hu et al., 2023) and report accuracy for all tasks. Each client has 1,000 training examples and 500 test examples. All federated baseline methods are trained for 600 communication rounds, while the local fine-tuning baseline is trained for 300 rounds to prevent overfitting. Since Fisher merging requires estimating Fisher information for all model parameters, it is computationally prohibitive for LLMs with over 1B parameters. In contrast, POTARA computes Fisher information only for the LoRA module, substantially reducing the number of parameters involved and making the computation tractable. For POTARA, we train FedIT for 50 rounds and local fine-tuning for 300 rounds, and then merge the resulting models to obtain the final personalized model for each client. As reported in Table 3, POTARA consistently outperforms all baselines across the evaluated NLP tasks. In particular, POTARA achieves the highest average accuracy, improving upon the strongest baseline by 1.85. Moreover, POTARA achieves these improvements with a very small communication overhead. See Section 4.3 and Figure 2b for a detailed performance-communication trade-off analysis. The gains observed across both large vision (ViT) and language models (LLaMA) demonstrate that POTARA generalizes well across model families, parameter scales, and task types.

Table 2. Test accuracy on personalized CIFAR-100 benchmark. POTARA obtains consistent improvement over the baselines across all clients.

Personalized CIFAR-100 benchmark (ViT-B/16 model)											
Methods	Client 1	Client 2	Client 3	Client 4	Client 5	Client 6	Client 7	Client 8	Client 9	Client 10	Avg.
Local	60.01 ±0.48	59.78 ±0.94	63.26 ±2.68	61.79 ±2.06	61.26 ±1.07	56.46 ±4.77	60.62 ±1.72	61.79 ±1.75	58.75 ±2.82	60.53 ±4.29	60.43 ±0.93
FFA-LoRA	39.96 ±3.87	44.55 ±2.91	42.36 ±6.53	40.14 ±2.98	42.85 ±1.62	38.62 ±0.80	41.50 ±3.63	40.03 ±2.37	44.07 ±1.86	41.08 ±6.12	41.52 ±2.44
FedSA	62.24 ±0.44	63.11 ±1.41	61.79 ±5.53	61.16 ±2.72	59.44 ±0.99	59.17 ±1.94	61.11 ±1.54	59.73 ±0.45	59.71 ±2.02	61.24 ±4.27	60.87 ±0.97
FedIT	62.55 ±2.33	60.53 ±2.37	60.30 ±4.86	59.48 ±3.38	62.07 ±3.63	59.99 ±1.51	61.93 ±3.14	62.73 ±1.52	63.60 ±3.15	59.61 ±3.35	61.28 ±0.29
FedDPA	62.80 ±1.46	60.51 ±2.79	61.22 ±4.81	62.41 ±2.87	61.54 ±2.43	60.31 ±1.71	63.24 ±1.94	62.09 ±2.13	62.74 ±1.82	61.14 ±4.61	61.80 ±0.96
Fish Merging	62.19 ±2.68	62.08 ±1.94	65.29 ±3.14	61.65 ±2.59	62.54 ±1.40	60.89 ±1.62	61.53 ±1.97	60.85 ±1.09	60.40 ±1.90	59.78 ±3.65	61.72 ±0.31
POTARA	66.32 ±1.11	66.55 ±0.94	67.26 ±4.70	63.43 ±1.79	65.86 ±1.39	62.93 ±0.28	66.37 ±1.76	64.60 ±1.20	65.15 ±0.76	63.68 ±3.34	65.21 ±1.08

Table 3. Test accuracy on commonsense reasoning benchmark. As in Table 2, POTARA obtains consistent improvements.

Commonsense reasoning benchmark (Llama-3.2-3B-Instruct model)									
Methods	ARC-c	ARC-e	BoolQ	HellaSwag	OBQA	PIQA	SIQA	WinoGrande	Avg.
Local	72.13 ±0.90	86.20 ±1.66	66.27 ±2.78	68.93 ±1.54	75.40 ±0.75	77.27 ±1.36	66.13 ±1.64	64.07 ±2.37	72.05 ±0.25
FFA-LoRA	73.27 ±0.50	85.53 ±0.52	64.80 ±0.91	57.73 ±2.78	73.87 ±0.50	79.07 ±1.52	62.00 ±7.09	54.13 ±1.18	68.80 ±0.77
FedSA	71.53 ±1.25	84.67 ±1.05	64.27 ±2.36	64.93 ±2.73	74.87 ±0.93	77.73 ±0.81	66.53 ±1.39	64.67 ±2.84	71.15 ±0.62
FedIT	74.27 ±0.62	85.93 ±1.46	66.87 ±1.18	64.93 ±1.05	74.33 ±1.64	78.80 ±1.77	69.87 ±1.09	60.53 ±1.75	71.94 ±0.42
FedALT	72.73 ±0.46	85.00 ±0.35	64.27 ±0.58	68.33 ±0.92	76.67 ±0.12	79.00 ±0.00	65.53 ±0.58	60.33 ±4.39	71.48 ±0.58
FedDPA	74.73 ±1.25	87.60 ±0.99	63.80 ±1.23	65.73 ±1.39	77.07 ±0.50	80.40 ±1.88	67.87 ±0.66	61.47 ±0.66	72.33 ±0.37
POTARA	75.20 ±1.28	87.80 ±1.31	67.87 ±0.57	71.73 ±2.23	78.47 ±1.04	78.80 ±2.36	69.00 ±1.18	64.53 ±2.00	74.18 ±0.29

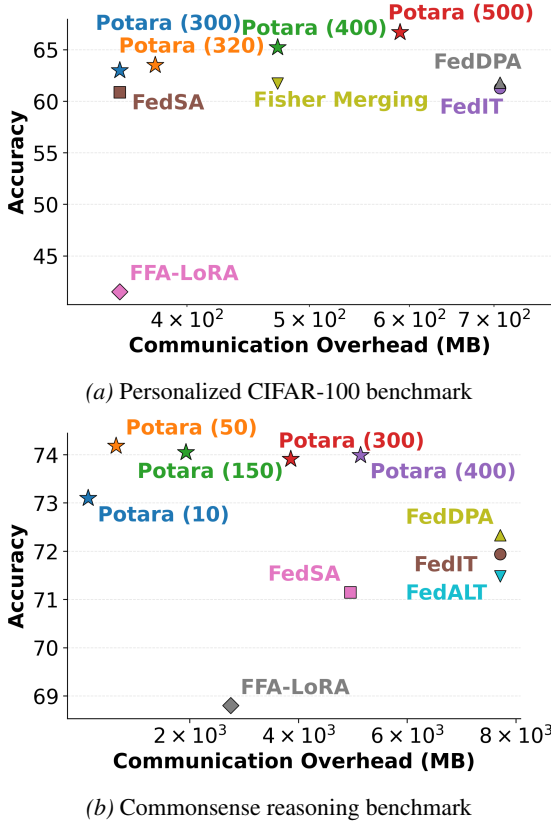


Figure 2. Performance-communication trade-off across different benchmarks. POTARA ( $t$ ) denotes our method where the FedIT model obtained at communication round  $t$  is used for merging. POTARA achieves strong performance with substantially lower communication overhead than baselines.

### 4.3. Performance-Communication Trade-Off

In this subsection, we compare the communication overhead of all methods. In ViT-B/16 model, the LoRA adaptation in-

troduces 147,456 parameters to the **A** matrices and 147,456 parameters to the **B** matrices, with each equivalent to 0.59 MB when stored in float32 precision. In LLaMa-3.2-3B-Instruct model, the LoRA adaptation introduces 2,064,384 parameters to the **A** matrices and 1,146,880 parameters to the **B** matrices, with equivalent to 8.26 MB and 4.59 MB when stored in float32 precision. POTARA ( $t$ ) denotes our method where the FedIT model obtained at communication round  $t$  is used for merging with the local model at round 300. Fig. 2 shows that POTARA consistently achieves the best performance-communication trade-off. In particular, POTARA attains the highest accuracy while requiring substantially less communication than FedIT, FedALT, and FedDPA. Moreover, compared to low-communication baselines, FedSA and FFA-LoRA, POTARA delivers clear performance gains at comparable overhead, demonstrating robust communication efficiency across different backbones and benchmarks.

### 4.4. Performance Gain of Model Merging

In this subsection, we show the performance gain by model merging over the FedIT and local models. Specifically, we compare the merged model POTARA with the FedIT model and the local model. For the vision benchmark, POTARA is obtained by merging the FedIT model trained for 400 rounds with the local model trained for 300 rounds. Table 4 shows that POTARA achieves 65.21 accuracy, improving the local baseline by 9.32 and the FedIT baseline by 7.33. For the commonsense reasoning benchmark, POTARA is obtained by merging the FedIT model trained for 50 rounds with the local model trained for 300 rounds. Table 5 shows that POTARA achieves 74.18 accuracy, improving the local baseline by 2.13 and the FedIT baseline by 6.45. These results indicate that model merging can effectively combine

Table 4. Performance gain of model merging under the personalized CIFAR-100 benchmark.

Model	Accuracy
Local (300 rounds)	55.89 ±1.31
FedIT (400 rounds)	57.88 ±0.38
POTARA	65.21 ±1.08

Table 5. Performance gain of model merging under the commonsense reasoning benchmark.

Model	Accuracy
Local (300 rounds)	72.05 ±0.25
FedIT (50 rounds)	67.73 ±0.76
POTARA	74.18 ±0.29

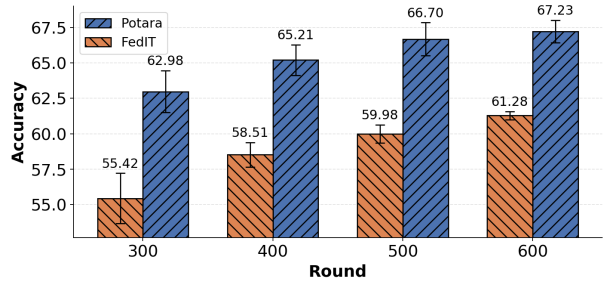
the global knowledge from FedIT model with the personalized knowledge from local fine-tuning model, leading to a substantial accuracy gain.

#### 4.5. Ablation Study

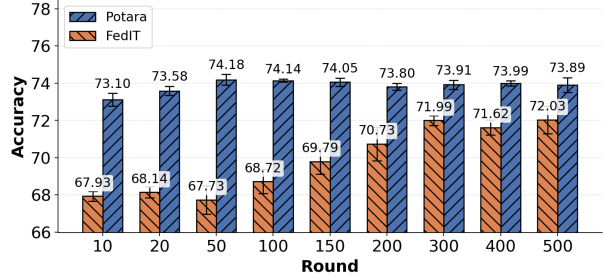
**Effect of FedIT model round for merging:** We examine the effect of the FedIT training round used for merging. Specifically, we fix the local fine-tuning model at round 300 and merge it with FedIT checkpoints trained for different numbers of rounds. As shown in Figure 3a and Figure 3b, POTARA improves steadily as the FedIT model is trained longer on both benchmarks, indicating that a better-optimized FedIT checkpoint provides stronger general knowledge that can be more effectively combined with the local model. On personalized CIFAR-100 benchmark (Figure 3a), increasing the FedIT training rounds yields a clear monotonic gain for the merged model (e.g., from 62.98 to 67.23). On the commonsense reasoning benchmark (Figure 3b), the merged model already achieves strong performance even when using an early FedIT checkpoint (e.g., round 50), despite the FedIT still improving substantially with more rounds. This suggests that POTARA can effectively extract useful general knowledge from intermediate FedIT models and combine it with local model.

**Effect of mixing weight strategy:** We compare client performance using the mixing weights computed by our method with the best-performing weights selected by grid search over  $\{0, 0.1, \dots, 1\}$ . As shown in Figure 3c, the two bars are closely matched across clients, demonstrating that our computed weights achieve performance comparable to grid search while eliminating the expensive per-client hyperparameter sweep. Moreover, Figure 3c supports our theory and assumptions as the mixing weights computed by our method are close to the empirically optimal weights found via grid search.

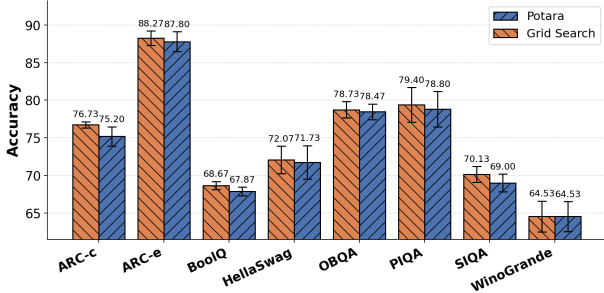
**Further experiments:** Results with an increased number of clients and with a larger model are reported in Appendix D and Appendix C, respectively.



(a) Effect of FedIT model round for merging (CIFAR-100).



(b) Effect of FedIT model round for merging (Commonsense Reasoning).



(c) Client performance comparison between mixing weights computed by our method and mixing weights selected by grid search.

Figure 3. Ablation studies demonstrating the performance of POTARA.

## 5. Conclusion

We proposed POTARA, a principled personalization framework for federated fine-tuning that merges a federated model and a local model. We approximate the federated and local task vectors as jointly Gaussian random variables and derive the upper bound on the expected excess task loss of the federated model, the local model, and their merged model, where the dominant term is a trace of the task vector variance. By minimizing this bound, we obtain closed-form optimal mixing weights, guaranteeing that the merged model attains a tighter bound than both constituent models. Experiment results show that POTARA consistently improves client performance across both vision and language benchmarks, outperforming baselines while retaining communication efficiency.

## Impact Statement

This paper makes important contributions to federated personalization by developing a principled framework for personalized fine-tuning. The focus of this work is on the technical advancement of large model fine-tuning. While this research has potential societal impacts, it primarily addresses technical challenges and does not necessitate a specific discussion on societal consequences.

## References

- Awais, M., Naseer, M., Khan, S., Anwer, R. M., Cholakkal, H., Shah, M., Yang, M.-H., and Khan, F. S. Foundation models defining a new era in vision: a survey and outlook. *IEEE Transactions on Pattern Analysis and Machine Intelligence*, 2025.
- Bai, J., Chen, D., Qian, B., Yao, L., and Li, Y. Federated fine-tuning of large language models under heterogeneous tasks and client resources. *Advances in Neural Information Processing Systems*, 2024.
- Bian, J., Wang, L., Zhang, L., and Xu, J. Fedalt: Federated fine-tuning through adaptive local training with rest-of-world lora. *AAAI Conference on Artificial Intelligence*, 2026.
- Carmon, Y., Duchi, J. C., Hinder, O., and Sidford, A. Accelerated methods for nonconvex optimization. *SIAM Journal on Optimization*, 28(2):1751–1772, 2018.
- Chen, F., Luo, M., Dong, Z., Li, Z., and He, X. Federated meta-learning with fast convergence and efficient communication. *arXiv preprint arXiv:1802.07876*, 2018.
- Chen, S., Zhou, T., Long, G., Jiang, J., and Zhang, C. Fed-merge: Federated personalization via model merging. *AAAI Conference on Artificial Intelligence*, 2026.
- Cho, Y. J., Liu, L., Xu, Z., Fahrezi, A., and Joshi, G. Heterogeneous lora for federated fine-tuning of on-device foundation models. *Conference on Empirical Methods in Natural Language Processing*, 2024.
- Chung, H. W., Hou, L., Longpre, S., Zoph, B., Tay, Y., Fedus, W., Li, Y., Wang, X., Dehghani, M., Brahma, S., et al. Scaling instruction-finetuned language models. *Journal of Machine Learning Research*, 25(70):1–53, 2024.
- Collins, L., Hassani, H., Mokhtari, A., and Shakkottai, S. Exploiting shared representations for personalized federated learning. *International Conference on Machine Learning*, 2021.
- Daxberger, E., Kristiadi, A., Immer, A., Eschenhagen, R., Bauer, M., and Hennig, P. Laplace redux-effortless bayesian deep learning. *Advances in Neural Information Processing Systems*, 2021.
- Dosovitskiy, A., Beyer, L., Kolesnikov, A., Weissenborn, D., Zhai, X., Unterthiner, T., Dehghani, M., Minderer, M., Heigold, G., and Gelly, S. An image is worth 16x16 words: Transformers for image recognition at scale. *International Conference on Learning Representations*, 2021.
- Draxler, F., Veschgini, K., Salmhofer, M., and Hamprecht, F. Essentially no barriers in neural network energy landscape. *International Conference on Machine Learning*, 2018.
- Duan, M., Liu, D., Ji, X., Wu, Y., Liang, L., Chen, X., Tan, Y., and Ren, A. Flexible clustered federated learning for client-level data distribution shift. *IEEE Transactions on Parallel and Distributed Systems*, 33(11):2661–2674, 2021.
- Dubey, A., Jauhri, A., Pandey, A., Kadian, A., Al-Dahle, A., Letman, A., Mathur, A., Schelten, A., Yang, A., Fan, A., et al. The llama 3 herd of models. *arXiv e-prints*, pp. arXiv–2407, 2024.
- Fallah, A., Mokhtari, A., and Ozdaglar, A. Personalized federated learning with theoretical guarantees: A model-agnostic meta-learning approach. *Advances in Neural Information Processing Systems*, 2020.
- Fang, W., Han, D.-J., Yuan, L., Hosseinalipour, S., and Brinton, C. G. Federated sketching lora: On-device collaborative fine-tuning of large language models. *arXiv preprint arXiv:2501.19389*, 2025.
- Fisher, R. A. On the mathematical foundations of theoretical statistics. *Philosophical transactions of the Royal Society of London. Series A, containing papers of a mathematical or physical character*, 222(594-604):309–368, 1922.
- Frankle, J., Dziugaite, G. K., Roy, D., and Carbin, M. Linear mode connectivity and the lottery ticket hypothesis. *International Conference on Machine Learning*, 2020.
- Garipov, T., Izmailov, P., Podoprikin, D., Vetrov, D. P., and Wilson, A. G. Loss surfaces, mode connectivity, and fast ensembling of dnns. *Advances in Neural Information Processing Systems*, 2018.
- Ghosh, A., Chung, J., Yin, D., and Ramchandran, K. An efficient framework for clustered federated learning. *Advances in Neural Information Processing Systems*, 2020.
- Guo, P., Zeng, S., Wang, Y., Fan, H., Wang, F., and Qu, L. Selective aggregation for low-rank adaptation in federated learning. *International Conference on Learning Representations*, 2025.
- Hao, J., Wu, Y., Payani, A., Lee, M., and Liu, M. Personalized federated fine-tuning for heterogeneous data: An automatic rank learning approach via two-level lora. *arXiv preprint arXiv:2503.03920*, 2025.

- Hayou, S., Ghosh, N., and Yu, B. Lora+: Efficient low rank adaptation of large models. *International Conference on Machine Learning*, 2024.
- Hu, E. J., Shen, Y., Wallis, P., Allen-Zhu, Z., Li, Y., Wang, S., Wang, L., Chen, W., et al. Lora: Low-rank adaptation of large language models. *International Conference on Learning Representations*, 2022.
- Hu, Z., Wang, L., Lan, Y., Xu, W., Lim, E.-P., Bing, L., Xu, X., Poria, S., and Lee, R. K.-W. Llm-adapters: An adapter family for parameter-efficient fine-tuning of large language models. *arXiv preprint arXiv:2304.01933*, 2023.
- Ilharco, G., Ribeiro, M. T., Wortsman, M., Gururangan, S., Schmidt, L., Hajishirzi, H., and Farhadi, A. Editing models with task arithmetic. *International Conference on Learning Representations*, 2023.
- Jin, X., Ren, X., Preotiuc-Pietro, D., and Cheng, P. Data-less knowledge fusion by merging weights of language models. *International Conference on Learning Representations*, 2023.
- Li, T., Hu, S., Beirami, A., and Smith, V. Ditto: Fair and robust federated learning through personalization. *International Conference on Machine Learning*, 2021.
- MacKay, D. J. A practical bayesian framework for backpropagation networks. *Neural computation*, 4(3):448–472, 1992.
- Matena, M. S. and Raffel, C. A. Merging models with fisher-weighted averaging. *Advances in Neural Information Processing Systems*, 2022.
- McMahan, B., Moore, E., Ramage, D., Hampson, S., and y Arcas, B. A. Communication-efficient learning of deep networks from decentralized data. In *Artificial intelligence and statistics*, pp. 1273–1282. PMLR, 2017.
- Nagarajan, V. and Kolter, J. Z. Uniform convergence may be unable to explain generalization in deep learning. *Advances in Neural Information Processing Systems*, 2019.
- Nesterov, Y. and Polyak, B. T. Cubic regularization of newton method and its global performance. *Mathematical programming*, 108(1):177–205, 2006.
- Neyshabur, B., Sedghi, H., and Zhang, C. What is being transferred in transfer learning? *Advances in Neural Information Processing Systems*, 2020.
- Pascanu, R. and Bengio, Y. Revisiting natural gradient for deep networks. *arXiv preprint arXiv:1301.3584*, 2013.
- Pillutla, K., Malik, K., Mohamed, A.-R., Rabbat, M., Sanjabi, M., and Xiao, L. Federated learning with partial model personalization. *International Conference on Machine Learning*, 2022.
- Qi, B., Sun, H., Long, W., Zhao, R., Gao, X., et al. Cabs: Conflict-aware and balanced sparsification for enhancing model merging. *International Conference on Learning Representations*, 2025.
- Qi, J., Luan, Z., Huang, S., Fung, C., Yang, H., and Qian, D. FDLORA: Personalized federated learning of large language model via dual lora tuning. *arXiv preprint arXiv:2406.07925*, 2024.
- Shamsian, A., Navon, A., Fetaya, E., and Chechik, G. Personalized federated learning using hypernetworks. *International Conference on Machine Learning*, 2021.
- Smith, V., Chiang, C.-K., Sanjabi, M., and Talwalkar, A. S. Federated multi-task learning. *Advances in Neural Information Processing Systems*, 2017.
- Stoica, G., Ramesh, P., Ecsedi, B., Choshen, L., and Hoffman, J. Model merging with svd to tie the knots. *International Conference on Learning Representations*, 2025.
- Sun, Y., Li, Z., Li, Y., and Ding, B. Improving loRA in privacy-preserving federated learning. *International Conference on Learning Representations*, 2024.
- Tam, D., Bansal, M., and Raffel, C. Merging by matching models in task parameter subspaces. *Transactions on Machine Learning Research*, 2024.
- Tan, A. Z., Yu, H., Cui, L., and Yang, Q. Towards personalized federated learning. *IEEE transactions on neural networks and learning systems*, 34(12):9587–9603, 2022.
- Tian, Z., Zhang, Z., Yang, Z., Jin, R., and Dai, H. Distributed learning over networks with graph-attention-based personalization. *IEEE Transactions on Signal Processing*, 71:2071–2086, 2023.
- Wang, Z., Shen, Z., He, Y., Sun, G., Wang, H., Lyu, L., and Li, A. Flora: Federated fine-tuning large language models with heterogeneous low-rank adaptations. *Advances in Neural Information Processing Systems*, 2024.
- Wang, Z., Xu, X., Liu, Y., Zhang, Y., Lin, P., Feng, S., Yang, X., Wang, D., and Schütze, H. Why do more experts fail? a theoretical analysis of model merging. *arXiv preprint arXiv:2505.21226*, 2025.
- Wortsman, M., Ilharco, G., Gadre, S. Y., Roelofs, R., Gontijo-Lopes, R., Morcos, A. S., Namkoong, H., Farhadi, A., Carmon, Y., Kornblith, S., et al. Model soups: averaging weights of multiple fine-tuned models improves accuracy without increasing inference time. *International Conference on Machine Learning*, 2022.
- Yadav, P., Tam, D., Choshen, L., Raffel, C. A., and Bansal, M. Ties-merging: Resolving interference when merging

- models. *Advances in Neural Information Processing Systems*, 2023.
- Yang, A., Li, A., Yang, B., Zhang, B., Hui, B., Zheng, B., Yu, B., Gao, C., Huang, C., Lv, C., et al. Qwen3 technical report. *arXiv preprint arXiv:2505.09388*, 2025.
- Yang, Y., Long, G., Shen, T., Jiang, J., and Blumenstein, M. Dual-personalizing adapter for federated foundation models. *Advances in Neural Information Processing Systems*, 2024.
- Yu, L., Yu, B., Yu, H., Huang, F., and Li, Y. Language models are super mario: Absorbing abilities from homologous models as a free lunch. *International Conference on Machine Learning*, 2024.
- Zhang, J., Vahidian, S., Kuo, M., Li, C., Zhang, R., Yu, T., Wang, G., and Chen, Y. Towards building the federatedgpt: Federated instruction tuning. In *ICASSP 2024-2024 IEEE International Conference on Acoustics, Speech and Signal Processing (ICASSP)*, pp. 6915–6919. IEEE, 2024.
- Zhao, W. X., Zhou, K., Li, J., Tang, T., Wang, X., Hou, Y., Min, Y., Zhang, B., Zhang, J., Dong, Z., et al. A survey of large language models. *arXiv preprint arXiv:2303.18223*, 1(2), 2023.
- Zhou, Z., Yang, Y., Yang, X., Yan, J., and Hu, W. Going beyond linear mode connectivity: The layerwise linear feature connectivity. *Advances in Neural Information Processing Systems*, 2023.

## A. Theoretical Results

### A.1. Derivation of Gaussian Distribution Approximation

The gaussian distribution approximation has been used in prior works (Matena & Raffel, 2022; Tam et al., 2024), but the full derivation is omitted. For completeness, we provide the full derivation.

The training of the individual task vector for task  $i$  can be formulated as a maximum a posteriori (MAP) estimation problem (Matena & Raffel, 2022; Wang et al., 2025) as follows

$$\boldsymbol{\mu}_i = \arg \max_{\boldsymbol{\theta}_i} p(\boldsymbol{\theta}_i | \mathcal{D}_i), \quad (21)$$

where  $\mathcal{D}_i$  denotes the dataset associated with task  $i$ . Here, task  $i$  may correspond either to the FedIT objective or to the local fine-tuning objective.

We perform a second-order Taylor expansion of the log-posterior around a point  $\hat{\boldsymbol{\theta}}$ :

$$\log p(\boldsymbol{\theta}_i | \mathcal{D}_i) \approx \log p(\hat{\boldsymbol{\theta}} | \mathcal{D}_i) + (\boldsymbol{\theta}_i - \hat{\boldsymbol{\theta}})^\top \nabla_{\boldsymbol{\theta}_i} \log p(\boldsymbol{\theta}_i | \mathcal{D}_i)|_{\boldsymbol{\theta}_i=\hat{\boldsymbol{\theta}}} - \frac{1}{2} (\boldsymbol{\theta}_i - \hat{\boldsymbol{\theta}})^\top \mathbf{H}_i (\boldsymbol{\theta}_i - \hat{\boldsymbol{\theta}}), \quad (22)$$

where  $\mathbf{H}_i = -\nabla_{\boldsymbol{\theta}_i}^2 \log p(\boldsymbol{\theta}_i | \mathcal{D}_i)|_{\boldsymbol{\theta}_i=\hat{\boldsymbol{\theta}}}$ .

We assume that the parameter  $\boldsymbol{\mu}_i$  of the trained neural network is a local maximum of the posterior distribution. By setting  $\hat{\boldsymbol{\theta}} = \boldsymbol{\mu}_i$ , we have  $\nabla_{\boldsymbol{\theta}_i} \log p(\boldsymbol{\theta}_i | \mathcal{D}_i)|_{\boldsymbol{\theta}_i=\boldsymbol{\mu}_i} = 0$ .

Then, we obtain

$$\log p(\boldsymbol{\theta}_i | \mathcal{D}_i) \approx \log p(\boldsymbol{\mu}_i | \mathcal{D}_i) - \frac{1}{2} (\boldsymbol{\theta}_i - \boldsymbol{\mu}_i)^\top \mathbf{H}_i (\boldsymbol{\theta}_i - \boldsymbol{\mu}_i), \quad (23)$$

where  $\mathbf{H}_i = -\nabla_{\boldsymbol{\theta}_i}^2 \log p(\boldsymbol{\theta}_i | \mathcal{D}_i)|_{\boldsymbol{\theta}_i=\boldsymbol{\mu}_i}$ .

Applying the Laplace approximation (MacKay, 1992; Daxberger et al., 2021) around the local optimum  $\boldsymbol{\mu}_i$ , the posterior distribution  $p(\boldsymbol{\theta}_i | \mathcal{D}_i)$  admits the following Gaussian approximation:

$$p(\boldsymbol{\theta}_i | \mathcal{D}_i) \approx \mathcal{N}(\boldsymbol{\theta}_i; \boldsymbol{\mu}_i, \mathbf{H}_i^{-1}) \quad (24)$$

Equivalently, we write

$$\boldsymbol{\theta}_i \sim \mathcal{N}(\boldsymbol{\mu}_i, \boldsymbol{\Sigma}_i) \quad \text{where } \boldsymbol{\Sigma}_i = \mathbf{H}_i^{-1}. \quad (25)$$

Given a trained neural network model  $p_{\boldsymbol{\mu}_i}(\mathbf{y} | \mathbf{x})$ , the Fisher information matrix (Matena & Raffel, 2022; Fisher, 1922) is defined as

$$\mathbf{F}_{\boldsymbol{\mu}_i} = \mathbb{E}_{\mathbf{x}} \left[ \mathbb{E}_{\mathbf{y} \sim p_{\boldsymbol{\mu}_i}(\mathbf{y} | \mathbf{x})} \left[ \nabla_{\boldsymbol{\mu}_i} \log p_{\boldsymbol{\mu}_i}(\mathbf{y} | \mathbf{x}) \nabla_{\boldsymbol{\mu}_i} \log p_{\boldsymbol{\mu}_i}(\mathbf{y} | \mathbf{x})^\top \right] \right]. \quad (26)$$

It can be shown that the Fisher information matrix coincides with the Hessian at modes of the distribution (Pascanu & Bengio, 2013).

### A.2. Proof of Theorem 3.6

Recall that the joint distribution of  $(\boldsymbol{\theta}_{\text{FedIT}}, \boldsymbol{\theta}_{\text{Local}})$  is given by

$$\begin{pmatrix} \boldsymbol{\theta}_{\text{FedIT}} \\ \boldsymbol{\theta}_{\text{Local}} \end{pmatrix} \sim \mathcal{N} \left( \begin{pmatrix} \boldsymbol{\mu}_{\text{FedIT}} \\ \boldsymbol{\mu}_{\text{Local}} \end{pmatrix}, \begin{pmatrix} \boldsymbol{\Sigma}_{\text{FedIT}} & \boldsymbol{\Sigma}_{\text{Cross}} \\ \boldsymbol{\Sigma}_{\text{Cross}}^\top & \boldsymbol{\Sigma}_{\text{Local}} \end{pmatrix} \right). \quad (27)$$

where  $\boldsymbol{\Sigma}_{\text{Cross}}$  denotes the cross-covariance between the two task vectors with  $\boldsymbol{\Sigma}_{\text{Cross}} \succeq \mathbf{0}$ ,  $\boldsymbol{\Sigma}_{\text{Cross}} \preceq \boldsymbol{\Sigma}_{\text{FedIT}}$  and  $\boldsymbol{\Sigma}_{\text{Cross}} \preceq \boldsymbol{\Sigma}_{\text{Local}}$ .

Then, the merged task vector follows the following Gaussian distribution:

$$\boldsymbol{\theta}_{\text{Merge}} \sim \mathcal{N}(\boldsymbol{\mu}_{\text{Merge}}, \boldsymbol{\Sigma}_{\text{Merge}}) \quad (28)$$

where

$$\boldsymbol{\mu}_{\text{merge}} = \lambda_{\text{FedIT}} \boldsymbol{\mu}_{\text{FedIT}} + \lambda_{\text{Local}} \boldsymbol{\mu}_{\text{Local}}, \quad (29)$$

$$\boldsymbol{\Sigma}_{\text{merge}} = \lambda_{\text{FedIT}}^2 \boldsymbol{\Sigma}_{\text{FedIT}} + \lambda_{\text{Local}}^2 \boldsymbol{\Sigma}_{\text{Local}} + \lambda_{\text{FedIT}} \lambda_{\text{Local}} (\boldsymbol{\Sigma}_{\text{Cross}} + \boldsymbol{\Sigma}_{\text{Cross}}^\top), \quad (30)$$

$$\lambda_{\text{FedIT}}, \lambda_{\text{Local}} \geq 0, \quad (31)$$

$$\lambda_{\text{FedIT}} + \lambda_{\text{Local}} = 1. \quad (32)$$

To analyze the effect of model merging, we expand the task loss  $\mathcal{L}$  around its optimum  $\mathbf{W}^*$ . Let  $\boldsymbol{\phi} = \mathbf{W}_{\text{Pre}} + \boldsymbol{\theta}_{\text{Merge}} - \mathbf{W}^*$  and  $\mathbf{H} = \nabla^2 \mathcal{L}(\mathbf{W}^*)$ , where  $\mathbf{W}_{\text{Pre}}$  is the pre-trained model that can be regarded as a constant vector. By Assumption 3.4 and Lemma 2.2 in (Carmon et al., 2018), we have

$$\mathcal{L}(\mathbf{W}_{\text{Pre}} + \boldsymbol{\theta}_{\text{Merge}}) \leq \mathcal{L}(\mathbf{W}^*) + \frac{1}{2} \boldsymbol{\phi}^\top \mathbf{H} \boldsymbol{\phi} + \frac{L_H}{6} \|\boldsymbol{\phi}\|_2^3. \quad (33)$$

By taking expectation, we obtain

$$\mathbb{E}[\mathcal{L}(\mathbf{W}_{\text{Pre}} + \boldsymbol{\theta}_{\text{Merge}}) - \mathcal{L}(\mathbf{W}^*)] \leq \frac{1}{2} \mathbb{E}[\boldsymbol{\phi}^\top \mathbf{H} \boldsymbol{\phi}] + \frac{L_H}{6} \mathbb{E}[\|\boldsymbol{\phi}\|_2^3]. \quad (34)$$

Using Lemma A.1 (i.e.,  $\mathbb{E}[\boldsymbol{\phi}^\top \mathbf{H} \boldsymbol{\phi}] = (\mathbb{E}\boldsymbol{\phi})^\top \mathbf{H} (\mathbb{E}\boldsymbol{\phi}) + \text{tr}(\mathbf{H} \text{Cov}(\boldsymbol{\phi}))$ ), we obtain

$$\begin{aligned} & \mathbb{E}[\mathcal{L}(\mathbf{W}_{\text{Pre}} + \boldsymbol{\theta}_{\text{Merge}}) - \mathcal{L}(\mathbf{W}^*)] \\ & \leq \frac{1}{2} \mathbb{E}[\boldsymbol{\phi}^\top \mathbf{H} \boldsymbol{\phi}] + \frac{L_H}{6} \mathbb{E}[\|\boldsymbol{\phi}\|_2^3] \\ & = \frac{1}{2} (\mathbb{E}\boldsymbol{\phi})^\top \mathbf{H} (\mathbb{E}\boldsymbol{\phi}) + \frac{1}{2} \text{tr}(\mathbf{H} \text{Cov}(\boldsymbol{\phi})) + \frac{L_H}{6} \mathbb{E}[\|\boldsymbol{\phi}\|_2^3] \\ & = \frac{1}{2} (\mathbf{W}_{\text{Pre}} + \boldsymbol{\mu}_{\text{Merge}} - \mathbf{W}^*)^\top \mathbf{H} (\mathbf{W}_{\text{Pre}} + \boldsymbol{\mu}_{\text{Merge}} - \mathbf{W}^*) + \frac{1}{2} \text{tr}(\mathbf{H} \boldsymbol{\Sigma}_{\text{Merge}}) + \frac{L_H}{6} \mathbb{E}[\|\boldsymbol{\phi}\|_2^3], \end{aligned} \quad (35)$$

where  $\boldsymbol{\mu}_{\text{Merge}} = \mathbb{E}[\boldsymbol{\theta}_{\text{Merge}}]$  and  $\boldsymbol{\Sigma}_{\text{Merge}} = \text{Cov}(\boldsymbol{\theta}_{\text{Merge}})$ .

By Assumption 3.2, we have  $\|\boldsymbol{\phi}\|_2 \leq \delta$ , and therefore  $\|\boldsymbol{\phi}\|_2^3 \leq \delta \|\boldsymbol{\phi}\|_2^2$ . Taking expectation yields  $\mathbb{E}[\|\boldsymbol{\phi}\|_2^3] \leq \delta \mathbb{E}[\|\boldsymbol{\phi}\|_2^2]$ . By the second-moment decomposition, we have

$$\mathbb{E}[\|\boldsymbol{\phi}\|_2^2] = \|\mathbb{E}\boldsymbol{\phi}\|_2^2 + \text{tr}(\text{Cov}(\boldsymbol{\phi})) = \|\mathbf{W}_{\text{Pre}} + \boldsymbol{\mu}_{\text{Merge}} - \mathbf{W}^*\|_2^2 + \text{tr}(\boldsymbol{\Sigma}_{\text{Merge}}). \quad (36)$$

Combining (35)–(36), we conclude that

$$\begin{aligned} \mathbb{E}[\mathcal{L}(\mathbf{W}_{\text{Pre}} + \boldsymbol{\theta}_{\text{Merge}}) - \mathcal{L}(\mathbf{W}^*)] & \leq \frac{1}{2} (\mathbf{W}_{\text{Pre}} + \boldsymbol{\mu}_{\text{Merge}} - \mathbf{W}^*)^\top \mathbf{H} (\mathbf{W}_{\text{Pre}} + \boldsymbol{\mu}_{\text{Merge}} - \mathbf{W}^*) + \frac{1}{2} \text{tr}(\mathbf{H} \boldsymbol{\Sigma}_{\text{Merge}}) \\ & \quad + \frac{L_H}{6} \delta \left( \|\mathbf{W}_{\text{Pre}} + \boldsymbol{\mu}_{\text{Merge}} - \mathbf{W}^*\|_2^2 + \text{tr}(\boldsymbol{\Sigma}_{\text{Merge}}) \right). \end{aligned} \quad (37)$$

Then, we have

$$\begin{aligned} \mathbb{E}[\mathcal{L}(\mathbf{W}_{\text{Pre}} + \boldsymbol{\theta}_{\text{Merge}}) - \mathcal{L}(\mathbf{W}^*)] & \leq \frac{L}{2} \|\mathbf{W}_{\text{Pre}} + \boldsymbol{\mu}_{\text{Merge}} - \mathbf{W}^*\|_2^2 + \frac{L}{2} \text{tr}(\boldsymbol{\Sigma}_{\text{Merge}}) \\ & \quad + \frac{L_H}{6} \delta \left( \|\mathbf{W}_{\text{Pre}} + \boldsymbol{\mu}_{\text{Merge}} - \mathbf{W}^*\|_2^2 + \text{tr}(\boldsymbol{\Sigma}_{\text{Merge}}) \right) \\ & \leq \frac{L}{2} \delta^2 + \frac{L}{2} \text{tr}(\boldsymbol{\Sigma}_{\text{Merge}}) + \frac{L_H}{6} \delta^3 + \frac{L_H}{6} \delta \text{tr}(\boldsymbol{\Sigma}_{\text{Merge}}) \\ & = \left( \frac{L}{2} + \frac{L_H}{6} \delta \right) \delta^2 + \left( \frac{L}{2} + \frac{L_H}{6} \delta \right) \text{tr}(\boldsymbol{\Sigma}_{\text{Merge}}) \end{aligned} \quad (38)$$

where the first inequality is due to Assumption 3.3, and the second inequality is due to Assumption 3.2.

Similarly, for each individual task vector we have

$$\mathbb{E}[\mathcal{L}(\mathbf{W}_{\text{Pre}} + \boldsymbol{\theta}_i) - \mathcal{L}(\mathbf{W}^*)] \leq \left( \frac{L}{2} + \frac{L_H}{6} \delta \right) \delta^2 + \left( \frac{L}{2} + \frac{L_H}{6} \delta \right) \text{tr}(\boldsymbol{\Sigma}_i), \quad i \in \{\text{FedIT}, \text{Local}\}. \quad (39)$$

### A.3. Proof of Lemma 3.7

Let

$$a = \text{tr}(\mathbf{\Sigma}_{\text{FedIT}}), \quad b = \text{tr}(\mathbf{\Sigma}_{\text{Local}}), \quad c = \text{tr}(\mathbf{\Sigma}_{\text{Cross}}). \quad (40)$$

Hence

$$\text{tr}(\mathbf{\Sigma}_{\text{Merge}}) = \text{tr}(\lambda_{\text{FedIT}}^2 \mathbf{\Sigma}_{\text{FedIT}} + \lambda_{\text{Local}}^2 \cdot \mathbf{\Sigma}_{\text{Local}} + \lambda_{\text{FedIT}} \lambda_{\text{Local}} (\mathbf{\Sigma}_{\text{Cross}} + \mathbf{\Sigma}_{\text{Cross}}^\top)) \quad (41)$$

$$= \lambda_{\text{FedIT}}^2 \cdot a + \lambda_{\text{Local}}^2 \cdot b + 2\lambda_{\text{FedIT}} \lambda_{\text{Local}} \cdot c \quad (42)$$

Using the Lemma A.2, we have

$$|c| = |\text{tr}(\mathbf{\Sigma}_{\text{Cross}})| \leq \sqrt{\text{tr}(\mathbf{\Sigma}_{\text{FedIT}}) \text{tr}(\mathbf{\Sigma}_{\text{Local}})} = \sqrt{ab}. \quad (43)$$

We define a function  $g(\cdot)$  with respect to  $\lambda_{\text{FedIT}}$  as follows

$$g(\lambda_{\text{FedIT}}) = \text{tr}(\mathbf{\Sigma}_{\text{Merge}}) = a\lambda_{\text{FedIT}}^2 + b(1 - \lambda_{\text{FedIT}})^2 + 2\lambda_{\text{FedIT}}(1 - \lambda_{\text{FedIT}})c, \quad (44)$$

where  $0 \leq \lambda_{\text{FedIT}} \leq 1$ .

This quadratic form is convex in  $\lambda_{\text{FedIT}}$ , because  $g''(\lambda_{\text{FedIT}}) = 2(a + b - 2c) \geq 2(a + b - 2\sqrt{ab}) = 2(\sqrt{a} - \sqrt{b})^2 \geq 0$ .

Then, we obtain the optimal  $\lambda_{\text{FedIT}}$  and the optimum as

$$\lambda_{\text{FedIT}}^* = \frac{b - c}{a + b - 2c} \in [0, 1], \quad (45)$$

$$g(\lambda_{\text{FedIT}}^*) = b - \frac{(b - c)^2}{a + b - 2c} = a - \frac{(a - c)^2}{a + b - 2c}. \quad (46)$$

Due to  $\mathbf{\Sigma}_{\text{Cross}} \preceq \mathbf{\Sigma}_{\text{FedIT}}$  and  $\mathbf{\Sigma}_{\text{Cross}} \preceq \mathbf{\Sigma}_{\text{Local}}$ , it follows that  $\text{tr}(\mathbf{\Sigma}_{\text{Cross}}) \leq \text{tr}(\mathbf{\Sigma}_{\text{FedIT}})$  and  $\text{tr}(\mathbf{\Sigma}_{\text{Cross}}) \leq \text{tr}(\mathbf{\Sigma}_{\text{Local}})$ . Combining both inequalities yields  $c \leq \min(a, b)$ . Therefore, the optimum is smaller than  $a$  and  $b$ , i.e.,  $g(\lambda_{\text{FedIT}}^*) \leq \min\{a, b\}$ .

So far, we have shown that, at the optimal mixing weights  $\lambda_{\text{FedIT}}^*$  and  $\lambda_{\text{Local}}^*$ ,  $\text{tr}(\mathbf{\Sigma}_{\text{Merge}})$  is smaller than  $\min\{\text{tr}(\mathbf{\Sigma}_{\text{FedIT}}), \text{tr}(\mathbf{\Sigma}_{\text{Local}})\}$ . Therefore, the merged model admits an excess loss upper bound that is tighter than the bounds for FedIT or local fine-tuning alone.

### A.4. Proof of Lemmas

**Lemma A.1.** Let  $\boldsymbol{\mu} = \mathbb{E}[\boldsymbol{\phi}]$  and  $\boldsymbol{\Sigma} = \text{Cov}(\boldsymbol{\phi}) = \mathbb{E}[(\boldsymbol{\phi} - \boldsymbol{\mu})(\boldsymbol{\phi} - \boldsymbol{\mu})^\top]$ . We have

$$\mathbb{E}[\boldsymbol{\phi}^\top \mathbf{H} \boldsymbol{\phi}] = (\mathbb{E} \boldsymbol{\phi})^\top \mathbf{H} (\mathbb{E} \boldsymbol{\phi}) + \text{tr}(\mathbf{H} \text{Cov}(\boldsymbol{\phi})) \quad (47)$$

*Proof.*

$$\begin{aligned} \mathbb{E}[\boldsymbol{\phi}^\top \mathbf{H} \boldsymbol{\phi}] &= \mathbb{E}[\text{tr}(\boldsymbol{\phi}^\top \mathbf{H} \boldsymbol{\phi})] = \mathbb{E}[\text{tr}(\mathbf{H} \boldsymbol{\phi} \boldsymbol{\phi}^\top)] = \text{tr}(\mathbf{H} \mathbb{E}[\boldsymbol{\phi} \boldsymbol{\phi}^\top]) \\ &= \text{tr}(\mathbf{H}(\boldsymbol{\Sigma} + \boldsymbol{\mu} \boldsymbol{\mu}^\top)) = \text{tr}(\mathbf{H} \boldsymbol{\Sigma}) + \text{tr}(\mathbf{H} \boldsymbol{\mu} \boldsymbol{\mu}^\top) \\ &= \text{tr}(\mathbf{H} \boldsymbol{\Sigma}) + \boldsymbol{\mu}^\top \mathbf{H} \boldsymbol{\mu} \end{aligned} \quad (48)$$

where we used  $\mathbb{E}[\boldsymbol{\phi} \boldsymbol{\phi}^\top] = \boldsymbol{\Sigma} + \boldsymbol{\mu} \boldsymbol{\mu}^\top$  and  $\text{tr}(\mathbf{A} \mathbf{B}) = \text{tr}(\mathbf{B} \mathbf{A})$ .  $\square$

**Lemma A.2.** Assume  $\begin{bmatrix} \boldsymbol{\Sigma}_1 & \boldsymbol{\Sigma}_{12} \\ \boldsymbol{\Sigma}_{12}^\top & \boldsymbol{\Sigma}_2 \end{bmatrix} \succeq 0$ . Then

$$|\text{tr}(\boldsymbol{\Sigma}_{12})| \leq \sqrt{\text{tr}(\boldsymbol{\Sigma}_1) \text{tr}(\boldsymbol{\Sigma}_2)} \quad (49)$$

*Proof.* Since  $\begin{bmatrix} \boldsymbol{\Sigma}_1 & \boldsymbol{\Sigma}_{12} \\ \boldsymbol{\Sigma}_{12}^\top & \boldsymbol{\Sigma}_2 \end{bmatrix} \succeq 0$ , there exists a matrix  $\mathbf{R}$  with  $\|\mathbf{R}\|_2 \leq 1$  such that

$$\boldsymbol{\Sigma}_{12} = \boldsymbol{\Sigma}_1^{1/2} \mathbf{R} \boldsymbol{\Sigma}_2^{1/2}. \quad (50)$$

By applying trace,

$$\text{tr}(\boldsymbol{\Sigma}_{12}) = \text{tr}(\boldsymbol{\Sigma}_1^{1/2} \mathbf{R} \boldsymbol{\Sigma}_2^{1/2}). \quad (51)$$

Using the trace inequality  $|\text{tr}(\mathbf{A}^\top \mathbf{B})| \leq \|\mathbf{A}\|_F \|\mathbf{B}\|_F$  and  $\|\mathbf{R}X\|_F \leq \|\mathbf{R}\|_2 \|X\|_F$ , we have

$$\begin{aligned} |\text{tr}(\boldsymbol{\Sigma}_{12})| &= |\text{tr}((\boldsymbol{\Sigma}_1^{1/2})^\top (\mathbf{R} \boldsymbol{\Sigma}_2^{1/2}))| \\ &\leq \|\boldsymbol{\Sigma}_1^{1/2}\|_F \|\mathbf{R} \boldsymbol{\Sigma}_2^{1/2}\|_F \\ &\leq \|\boldsymbol{\Sigma}_1^{1/2}\|_F \|\mathbf{R}\|_2 \|\boldsymbol{\Sigma}_2^{1/2}\|_F \\ &\leq \|\boldsymbol{\Sigma}_1^{1/2}\|_F \|\boldsymbol{\Sigma}_2^{1/2}\|_F. \end{aligned} \quad (52)$$

Note that  $\|\boldsymbol{\Sigma}_1^{1/2}\|_F^2 = \text{tr}((\boldsymbol{\Sigma}_1^{1/2})^\top \boldsymbol{\Sigma}_1^{1/2}) = \text{tr}(\boldsymbol{\Sigma}_1^{1/2} \boldsymbol{\Sigma}_1^{1/2}) = \text{tr}(\boldsymbol{\Sigma}_1)$ . Similarly,  $\|\boldsymbol{\Sigma}_2^{1/2}\|_F^2 = \text{tr}(\boldsymbol{\Sigma}_2)$ . Therefore,

$$|\text{tr}(\boldsymbol{\Sigma}_{12})| \leq \sqrt{\text{tr}(\boldsymbol{\Sigma}_1) \text{tr}(\boldsymbol{\Sigma}_2)}.$$

□

## B. Implementation

Let  $\{(\mathbf{x}_n, \mathbf{y}_n)\}_{n=1}^N$  be a random data batch from training set of client  $i$ . For two well-trained models with parameters  $\boldsymbol{\mu}_{\text{FedIT}}$  and  $\boldsymbol{\mu}_{\text{Local}}$ , the per-sample gradients are given by

$$\mathbf{g}_{\text{FedIT}}^{(n)} \triangleq \nabla_{\boldsymbol{\mu}_{\text{FedIT}}} \ell(\boldsymbol{\mu}_{\text{FedIT}}; \mathbf{x}_n, \mathbf{y}_n), \quad \mathbf{g}_{\text{Local}}^{(n)} \triangleq \nabla_{\boldsymbol{\mu}_{\text{Local}}} \ell(\boldsymbol{\mu}_{\text{Local}}; \mathbf{x}_n, \mathbf{y}_n), \quad (53)$$

where  $\ell$  is the per-sample task loss. For each parameter coordinate  $k \in \{1, \dots, d\}$ , compute the mean and variance of per-sample gradient, and covariance as

$$\bar{g}_{\text{FedIT},k} = \frac{1}{N} \sum_{n=1}^N g_{\text{FedIT},k}^{(n)}, \quad \bar{g}_{\text{Local},k} = \frac{1}{N} \sum_{n=1}^N g_{\text{Local},k}^{(n)}, \quad (54)$$

$$\text{Var}_{\text{FedIT}}(k) = \frac{1}{N} \sum_{n=1}^N (g_{\text{FedIT},k}^{(n)} - \bar{g}_{\text{FedIT},k})^2, \quad \text{Var}_{\text{Local}}(k) = \frac{1}{N} \sum_{n=1}^N (g_{\text{Local},k}^{(n)} - \bar{g}_{\text{Local},k})^2, \quad (55)$$

$$\text{Cov}_{\text{Cross}}(k) = \frac{1}{N} \sum_{n=1}^N (g_{\text{FedIT},k}^{(n)} - \bar{g}_{\text{FedIT},k})(g_{\text{Local},k}^{(n)} - \bar{g}_{\text{Local},k}). \quad (56)$$

The gradient correlation coefficient for coordinate  $k$  is defined as

$$\rho_k \triangleq \frac{\text{Cov}_{\text{Cross}}(k)}{\sqrt{\text{Var}_{\text{FedIT}}(k) \text{Var}_{\text{Local}}(k)}}, \quad \rho_k \in [-1, 1]. \quad (57)$$

We adopt a diagonal approximation for the cross-covariance,

$$(\boldsymbol{\Sigma}_{\text{Cross}})_{kk} \triangleq \rho_k \sqrt{(\boldsymbol{\Sigma}_{\text{FedIT}})_{kk} (\boldsymbol{\Sigma}_{\text{Local}})_{kk}}, \quad k = \{1, \dots, d\},$$

and clip  $\rho_k$  to ensure  $\boldsymbol{\Sigma}_{\text{Cross}} \succeq 0$  and  $\boldsymbol{\Sigma}_{\text{Cross}} \preceq \boldsymbol{\Sigma}_{\text{FedIT}}, \boldsymbol{\Sigma}_{\text{Local}}$ :

$$\rho_k \triangleq \max\{0, \min\{\rho_k, \rho_k^{\max}\}\}, \quad \text{where } \rho_k^{\max} = \min\left\{\sqrt{\frac{(\boldsymbol{\Sigma}_{\text{FedIT}})_{kk}}{(\boldsymbol{\Sigma}_{\text{Local}})_{kk}}}, \sqrt{\frac{(\boldsymbol{\Sigma}_{\text{Local}})_{kk}}{(\boldsymbol{\Sigma}_{\text{FedIT}})_{kk}}}\right\}. \quad (58)$$

This yields a PSD diagonal  $\boldsymbol{\Sigma}_{\text{Cross}}$  with each element bounded by the corresponding entries of  $\boldsymbol{\Sigma}_{\text{FedIT}}$  and  $\boldsymbol{\Sigma}_{\text{Local}}$ .

Then, we calculate the scalar  $c$  as

$$c \triangleq \text{tr}(\boldsymbol{\Sigma}_{\text{Cross}}) = \sum_{k=1}^d (\boldsymbol{\Sigma}_{\text{Cross}})_{kk} = \sum_{k=1}^d \rho_k \sqrt{(\boldsymbol{\Sigma}_{\text{FedIT}})_{kk} (\boldsymbol{\Sigma}_{\text{Local}})_{kk}} \quad (59)$$

Note that in practice  $\boldsymbol{\theta}$  is parameterized by LoRA modules  $\{\mathbf{B}, \mathbf{A}\}$  and the actual trainable parameters are  $\mathbf{B}$  and  $\mathbf{A}$ . Therefore, the Fisher information matrix in Eq. (19) is estimated with respect to the LoRA parameters  $\{\mathbf{B}, \mathbf{A}\}$  rather than the composed matrix product  $\mathbf{BA}$ . Accordingly, we estimate the diagonal Fisher information for  $\mathbf{B}$  and  $\mathbf{A}$ , and perform merging separately for  $\mathbf{B}$  and  $\mathbf{A}$ , instead of first forming  $\boldsymbol{\theta} = \mathbf{BA}$  and computing its Fisher information.

## C. Experiments on FLAN benchmark

### C.1. Performance Comparison

We evaluate POTARA on the FLAN benchmark (Chung et al., 2024), which consists of over 60 datasets covering more than 12 NLP task categories. To simulate an extreme heterogeneity scenario, we consider eight clients, each trained on a completely different dataset. This setting is highly task-heterogeneous and is substantially more extreme than the CIFAR-100 and commonsense reasoning setups. Dataset details, task descriptions, and client assignments are summarized in Appendix C.2. We adopt Qwen3-4B-Instruct-2507 (Yang et al., 2025) as the pre-trained model and report ROUGE-1 for all tasks. Baselines are trained for 600 rounds, except local fine-tuning which runs for 300 rounds to mitigate overfitting. For POTARA, we train FedIT for 300 rounds and local fine-tuning for 300 rounds, and merge the two resulting models to obtain the final model. As shown in Table 6, POTARA achieves the best overall ROUGE-1 on the FLAN benchmark and consistently performing strongly across diverse task categories, indicating that merging global knowledge with personalized knowledge is especially effective under extreme task heterogeneity. Meanwhile, POTARA attains these improvements while reducing communication cost because it merges an intermediate FedIT model with local model.

Table 6. ROUGE-1 performance on FLAN benchmark (Qwen3-4B-Instruct model).

FLAN benchmark (Qwen3-4B-Instruct model)									
Methods	Closed-book QA	Reading Comp.	Coreference	Paraphrase	Commonsense	NLI	Reading	Sentiment	Avg.
Local	69.53 $\pm$ 0.75	69.38 $\pm$ 2.81	88.01 $\pm$ 0.70	80.00 $\pm$ 3.56	87.62 $\pm$ 0.78	85.78 $\pm$ 2.18	73.87 $\pm$ 0.66	76.16 $\pm$ 1.69	78.79 $\pm$ 0.99
FFA-LoRA	71.00 $\pm$ 0.66	70.54 $\pm$ 0.66	77.18 $\pm$ 1.34	79.89 $\pm$ 0.57	85.65 $\pm$ 1.18	86.33 $\pm$ 1.18	73.57 $\pm$ 0.39	77.06 $\pm$ 0.74	77.65 $\pm$ 0.70
FedSA	69.54 $\pm$ 0.95	69.54 $\pm$ 1.09	87.78 $\pm$ 2.61	81.89 $\pm$ 0.87	84.05 $\pm$ 1.16	86.00 $\pm$ 1.19	72.72 $\pm$ 0.65	76.47 $\pm$ 0.98	78.50 $\pm$ 0.25
FedIT	69.96 $\pm$ 0.57	71.37 $\pm$ 0.63	83.19 $\pm$ 0.51	80.44 $\pm$ 1.40	85.37 $\pm$ 0.96	86.33 $\pm$ 1.25	73.78 $\pm$ 0.85	76.68 $\pm$ 0.56	78.39 $\pm$ 0.63
FedDPA	70.03 $\pm$ 0.19	70.57 $\pm$ 0.34	81.89 $\pm$ 1.37	81.44 $\pm$ 0.79	86.93 $\pm$ 1.71	87.55 $\pm$ 0.88	74.01 $\pm$ 0.02	76.45 $\pm$ 0.88	78.61 $\pm$ 0.29
FedALT	68.07 $\pm$ 1.51	72.50 $\pm$ 0.77	84.84 $\pm$ 0.51	82.44 $\pm$ 1.03	85.17 $\pm$ 0.07	86.78 $\pm$ 0.57	73.43 $\pm$ 0.86	77.40 $\pm$ 1.02	78.83 $\pm$ 0.26
POTARA	70.61 $\pm$ 0.54	70.61 $\pm$ 2.06	88.26 $\pm$ 1.77	81.56 $\pm$ 0.42	88.80 $\pm$ 0.23	86.78 $\pm$ 1.10	75.18 $\pm$ 0.78	76.10 $\pm$ 1.01	79.74 $\pm$ 0.27

### C.2. FLAN benchmark

We follow the experimental setup in (Bian et al., 2026; Yang et al., 2024) to simulate a client-level task heterogeneity setting using the FLAN datasets (Chung et al., 2024). The FLAN collection comprises over 12 natural language processing tasks, each of which contains multiple datasets. These tasks are generated from diverse contextual factors and inherently exhibit complex and heterogeneous data distribution shifts. We consider an extreme client heterogeneity setting where 8 clients are assigned completely different NLP tasks. To simulate a realistic environment where each client has limited access to large-scale datasets, we adopt a downsampling strategy that assigns 2000 training samples and 300 test samples to each client. The specific task and dataset assignments are summarized in Table 7.

Table 7. FLAN benchmark.

Task	Dataset	Description
Closed-book QA	arc_challenge	Answer multiple-choice questions.
Reading Comp. w/ Commonsense	cosmos_qa	Reading comprehension with commonsense.
Coreference Resolution	definite_pronoun_resolution	Resolve ambiguous pronouns.
Paraphrase Detection	glue_qqp	Identify semantic equivalence.
Commonsense Reasoning	hellaswag	Choose the most plausible continuation.
Natural Language Inference	mnli	Infer relations between sentence pairs.
Reading Comprehension	squad_v1	Extract answers from passages.
Sentiment Analysis	sst2	Sentence-level sentiment classification.

### D. Experiments with Increased Number of Clients

In this section, we extend our experiments to settings with a larger number of clients. For the personalized CIFAR-100 benchmark, we increase the number of clients to 20, with each client following a distinct label distribution. For the commonsense reasoning benchmark, we increase the number of clients to 16, where every two clients share the same task but have different training samples. Table 8 and 9 show that with increased number of clients, POTARA consistently outperforms all baselines, demonstrating robust performance gains at larger scale.

Table 8. Testing accuracy on personalized CIFAR-100 benchmark with 20 clients.

Client	Local	FFA-LoRA	FedSA	FedIT	FedDPA	Fisher Merging	POTARA
Client 1	63.53 ±2.22	44.37 ±1.97	61.28 ±2.27	59.52 ±0.73	67.41 ±2.92	62.00 ±2.46	62.39 ±3.91
Client 2	62.28 ±5.39	49.25 ±6.36	61.16 ±5.72	61.35 ±6.12	65.95 ±6.74	61.39 ±9.09	70.18 ±5.12
Client 3	60.40 ±0.23	45.24 ±1.43	58.25 ±2.07	64.25 ±2.42	65.39 ±3.34	59.64 ±2.42	70.09 ±1.34
Client 4	58.45 ±2.62	39.74 ±0.34	57.29 ±1.19	56.98 ±2.56	59.52 ±0.55	62.54 ±0.71	63.63 ±1.26
Client 5	62.07 ±2.18	50.88 ±4.72	62.73 ±2.31	66.00 ±3.74	68.64 ±1.89	66.22 ±0.01	67.94 ±4.36
Client 6	64.14 ±0.67	47.09 ±2.28	61.07 ±0.85	65.06 ±2.94	65.34 ±2.65	59.56 ±0.25	67.00 ±0.09
Client 7	58.82 ±0.95	40.24 ±1.49	58.12 ±0.59	57.96 ±1.45	58.85 ±3.59	61.12 ±2.24	61.66 ±0.95
Client 8	62.78 ±1.61	44.65 ±0.02	59.21 ±0.43	63.37 ±3.22	64.41 ±1.21	63.31 ±0.11	65.35 ±2.42
Client 9	62.58 ±1.40	42.76 ±2.31	60.06 ±1.32	59.63 ±4.14	60.85 ±3.94	65.22 ±0.23	66.83 ±0.98
Client 10	62.14 ±1.33	44.13 ±2.60	59.58 ±4.50	62.31 ±2.31	65.35 ±1.79	62.25 ±0.61	66.92 ±1.45
Client 11	60.16 ±1.79	44.74 ±1.14	59.23 ±2.08	64.24 ±1.03	62.61 ±1.03	57.62 ±0.73	61.96 ±0.85
Client 12	57.86 ±1.87	44.80 ±2.32	55.35 ±0.39	65.66 ±1.49	60.01 ±0.94	59.58 ±2.15	63.40 ±1.89
Client 13	61.04 ±1.68	46.04 ±7.54	61.00 ±1.22	61.74 ±1.95	64.73 ±3.67	60.20 ±4.24	66.48 ±1.17
Client 14	60.64 ±2.41	43.08 ±1.47	58.89 ±4.14	60.73 ±3.29	59.39 ±8.12	64.56 ±4.91	63.97 ±4.32
Client 15	59.61 ±1.47	37.66 ±0.69	57.57 ±1.00	61.24 ±1.12	60.62 ±2.62	59.30 ±1.39	63.62 ±2.54
Client 16	57.85 ±0.45	42.66 ±0.24	57.34 ±0.59	60.27 ±3.41	58.12 ±0.53	59.75 ±2.71	63.39 ±1.66
Client 17	62.09 ±4.21	43.70 ±8.42	58.79 ±2.54	64.45 ±5.90	61.59 ±4.52	63.83 ±3.02	64.84 ±3.86
Client 18	58.45 ±2.12	43.16 ±0.08	57.26 ±0.93	59.52 ±0.82	57.10 ±1.57	59.87 ±3.55	64.88 ±2.82
Client 19	62.75 ±3.68	50.26 ±1.38	63.88 ±1.85	66.43 ±1.42	66.52 ±2.21	66.39 ±2.62	71.42 ±0.54
Client 20	58.68 ±0.28	43.53 ±2.69	60.81 ±0.45	63.67 ±3.51	62.98 ±1.16	60.39 ±2.02	67.26 ±0.28
<b>Average</b>	60.81 ±0.57	44.40 ±1.09	59.45 ±0.95	62.22 ±0.93	62.77 ±0.63	61.73 ±1.45	65.66 ±0.82

Table 9. Testing accuracy on commonsense reasoning benchmark with 16 clients.

Client	Local	FFA-LoRA	FedSA	FedIT	FedALT	FedDPA	POTARA
Client 1 (ARC-c)	71.80 ±0.20	73.00 ±0.80	70.60 ±0.40	73.60 ±0.00	73.50 ±0.70	74.50 ±0.90	74.80 ±0.20
Client 2 (ARC-c)	70.50 ±0.50	73.10 ±0.30	72.20 ±1.20	73.60 ±0.00	72.40 ±0.00	74.50 ±0.10	75.20 ±1.00
Client 3 (ARC-e)	85.80 ±0.20	87.50 ±0.50	86.20 ±1.20	87.30 ±0.70	85.90 ±0.70	86.90 ±0.30	88.50 ±0.30
Client 4 (ARC-e)	86.70 ±0.50	87.10 ±0.50	85.90 ±1.30	87.30 ±0.70	85.00 ±0.20	87.40 ±0.60	87.90 ±0.30
Client 5 (BoolQ)	65.20 ±3.00	67.00 ±0.60	61.60 ±5.60	64.30 ±3.50	66.70 ±0.10	66.90 ±0.10	65.60 ±0.60
Client 6 (BoolQ)	67.90 ±1.50	63.50 ±1.70	64.90 ±0.70	64.30 ±3.50	65.50 ±0.30	64.20 ±3.00	66.70 ±1.70
Client 7 (HellaSwag)	68.50 ±1.50	58.50 ±0.10	66.70 ±1.90	66.90 ±1.10	69.00 ±0.20	65.00 ±0.00	69.70 ±1.30
Client 8 (HellaSwag)	68.10 ±0.10	59.70 ±0.50	63.90 ±2.50	66.90 ±1.10	68.00 ±1.20	68.10 ±0.70	68.30 ±0.90
Client 9 (OBQA)	75.90 ±0.50	71.30 ±2.90	72.90 ±0.30	76.70 ±0.10	75.80 ±1.00	78.00 ±1.80	78.70 ±0.50
Client 10 (OBQA)	74.90 ±2.50	73.80 ±0.40	73.50 ±1.30	76.70 ±0.10	76.00 ±1.00	77.80 ±1.00	77.90 ±0.70
Client 11 (PIQA)	80.20 ±0.80	79.40 ±1.80	77.40 ±0.40	80.60 ±0.60	79.80 ±0.20	80.20 ±0.60	81.90 ±0.90
Client 12 (PIQA)	79.40 ±1.00	77.60 ±2.60	78.30 ±0.70	80.60 ±0.60	79.20 ±1.60	81.20 ±0.60	81.90 ±0.30
Client 13 (SIQA)	67.70 ±1.10	67.60 ±0.20	67.00 ±0.80	70.50 ±0.10	70.80 ±3.00	71.30 ±1.50	73.00 ±1.60
Client 14 (SIQA)	67.80 ±1.20	67.70 ±0.70	68.30 ±0.70	70.50 ±0.10	66.50 ±0.50	69.20 ±1.80	72.40 ±1.80
Client 15 (WinoGrande)	67.00 ±0.20	52.20 ±2.60	66.20 ±0.40	62.00 ±0.80	63.40 ±0.00	62.10 ±0.50	62.80 ±0.60
Client 16 (WinoGrande)	64.80 ±1.00	51.30 ±1.70	64.30 ±1.30	62.00 ±0.80	63.20 ±0.40	61.70 ±0.10	63.60 ±0.20
<b>Average</b>	72.64 ±0.34	69.39 ±0.38	71.25 ±0.35	72.74 ±0.24	72.55 ±0.53	73.06 ±0.23	74.31 ±0.58

### E. Client Performance with Various Mixing Weight

In this section, we investigate the effect of the mixing weight  $\lambda$  that balances the FedIT model and the local fine-tuning model in the proposed POTARA framework. Specifically, we vary  $\lambda \in \{0, 0.1, \dots, 1\}$  and evaluate client-wise performance under different mixing weights, where  $\lambda = 1$  corresponds to using the FedIT model alone and  $\lambda = 0$  corresponds to

purely local fine-tuning. We conduct this analysis on commonsense reasoning benchmark with LLaMA. Figure 4 shows that the performance of nearly all clients exhibits a clear unimodal trend with respect to  $\lambda$ , with intermediate mixing weights outperforming both extreme settings. This observation confirms that neither purely general knowledge nor purely personalized knowledge is sufficient, and that an appropriate combination of the two yields superior performance. Moreover, as the FedIT model is trained for more communication rounds, the peak of the unimodal curves shifts noticeably toward larger  $\lambda$  for nearly all clients. Consistently, the mixing weights estimated by our method (indicated by red dashed lines) also move to the right as the FedIT round increases. This behavior indicates that a better-trained FedIT model contributes more reliable general knowledge to the merged model. This rightward shift further suggests that the Fisher information associated with the FedIT model increases as training proceeds, which in turn assigns a larger weight to the FedIT model during model merging.

### F. Computation Time

We report the computation time required to compute the mixing weights on three benchmarks, as well as the training time of the FedIT model and the local model on the same benchmarks. We randomly sample 30 data samples from the training set of each client. As shown in Table 10, the computation time for mixing weights is modest compared to the overall training cost. Notably, this procedure is executed only once and does not introduce additional per-round communication or optimization overhead in the federated learning process.

Table 10. Computation time and training time.

Task	Pre-trained Model	Mixing Weights Computation Time	FedIT + Local Training Time
CIFAR-100	ViT-B/16	52.06s	0.83h
Commonsense Reasoning	LLaMA-3.2-3B	0.46h	5.92h
FLAN	Qwen3-4B-Instruct-2507	1.18h	6.83h

### G. Hyperparameters

Unless stated otherwise, the hyperparameters used in this work are as follows.

Table 11. Hyperparameter setting.

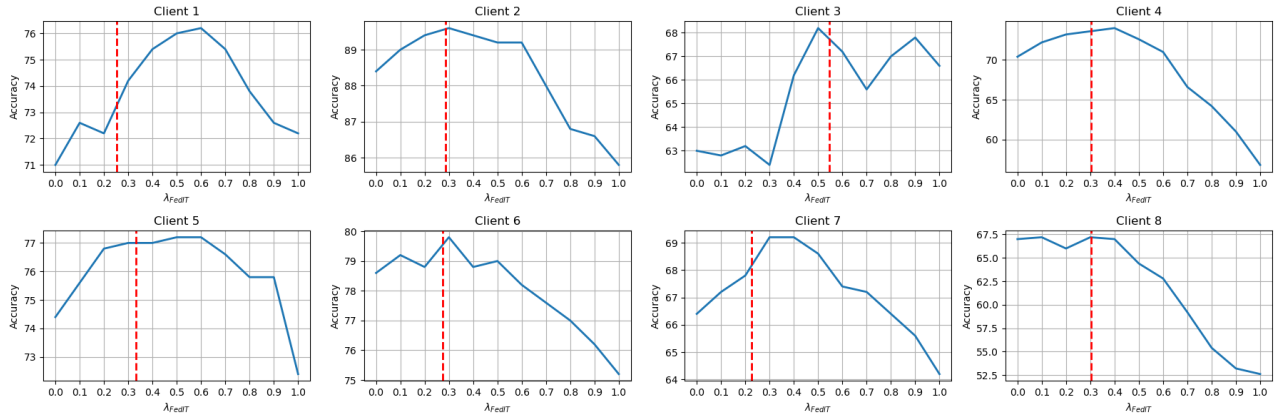
Hyperparameter	ViT-B/16 & CIFAR-100	LLaMA-3.2-3B-Instruct & commonsense reasoning	Qwen3-4B-Instruct-2507 & FLAN
Batch size	10	4	4
Learning rate	0.001	0.0001	0.0001
LoRA dropout rate	0.1	0.05	0.05
Local iteration number	5	4	4
Target module	["query", "value"]	["q_proj", "k_proj", "v_proj"]	["q_proj", "k_proj", "v_proj"]
Number of data samples to compute mixing weights	30	30	30

### H. Difference between Fisher Merging and POTARA

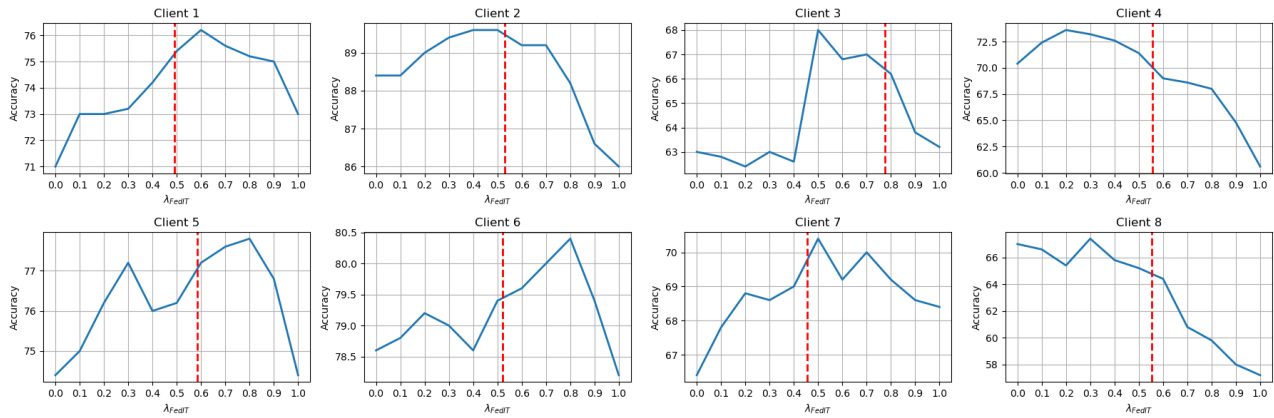
Our proposed method POTARA differs from Fisher merging in two fundamental aspects.

First, these two methods operate in different parameter spaces, which leads to vastly different computational costs. Fisher merging is performed in the full parameter space of the model. When the model size is small (e.g., fewer than hundred million parameters), the computation of the Fisher information matrix is manageable and does not introduce significant overhead. However, for LLMs, whose parameter size typically exceeds one billion, computing the Fisher information for all parameters becomes computationally prohibitive. In contrast, our method performs merging in the task vector space and computes the Fisher information only for the LoRA parameters, whose dimensionality is several orders of magnitude smaller than that of the full model. As a result, our approach incurs substantially lower computational overhead and remains practical for LLMs.

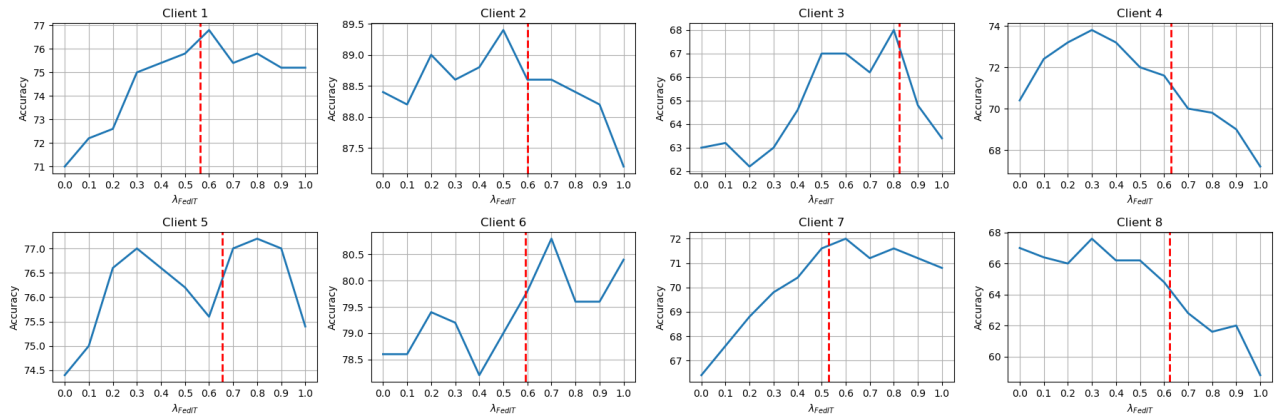
Second, Fisher merging assumes independence between the models being merged and ignores their correlation structure. Specifically, Fisher merging combines models by weighting them according to their individual Fisher information matrices, without considering correlation between models. In contrast, our method explicitly models the correlation between the federated model and the local model, which allows us to derive a more principled and optimal mixing weight.



(a) Merging FedIT model at round 50 with local model at round 300 under varying mixing weight.



(b) Merging FedIT model at round 150 with local model at round 300 under varying mixing weight.



(c) Merging FedIT model at round 300 with local model at round 300 under varying mixing weight.

Figure 4. Client performance under various mixing weights. For each client, we construct a personalized model by merging a FedIT checkpoint at round 50, 150, or 300 with a fixed Local model at round 300, and sweep the local mixing weight  $\lambda_{\text{FedIT}}$  (x-axis). Curves report the resulting client accuracy. The red dashed line marks the mixing weight calculated by our method for each client.